Journal of Geochemical Exploration 220 (2021) 106676

Contents lists available at ScienceDirect

Journal of Geochemical Exploration

journal homepage: www.elsevier.com/locate/gexplo

Geochemistry of the Yudong bauxite deposit, south-eastern Guizhou, China: Implications for conditions of formation and parental affinity

Jiafei Xiao *, Yantao Li, Haiying Yang, Jianbin Xu, Mingliang Huang

State Key Laboratory of Ore Deposit Geochemistry, Institute of Geochemistry Chinese Academy of Sciences, Guiyang 550081, China

ARTICLE INFO

Keywords:
Bauxite
Geochemistry
Formation conditions
Parental affinity
South-eastern Guizhou

ABSTRACT

The Yudong bauxite deposit is located in the Kaili–Huangping bauxite-concentrated area, in south-eastern Guizhou Province, China. The ore-bearing rock series consists of the lower part (Fe-bearing member) and middle part (Al-bearing member) of the Middle Permian Liangshan Formation, covering the Upper Devonian Gaopochang Formation. The elemental content in the ore-bearing profile is variable. In general, Al, Ti, V, Cr, Zr, Nb, Hf, Th, and U increase from the Fe- to the Al-bearing member, whereas Si, Fe, Rb, Cs, Ba, and total rare earth elements (REE) decrease. These observations indicate the occurrence of bauxitisation, which corresponds to a process of elemental variation during which Si and Fe were dissolved and migrated, and Al was enriched. Compared with Ordovician–Silurian (O–S) mudrock, the ore-bearing rock series are enriched in Al, Ti, V, Zr, Hf, Nb, Ta, Th, and U, but depleted in Si, Fe, Rb, Cs, and Ba as a result of weathering. The REEs show negative correlations with Si, Fe, K, Na, Ca, Mg, and Y, indicating that the REEs may be associated with clay, Fe-bearing, and Y-bearing minerals.

The La/Y ratio, $(La/Yb)_N$ ratio, and Ce anomalies show that the Fe-bearing member formed in an alkaline reducing environment, whereas the Al-bearing member formed in an acidic oxic environment. The immobile element ratios, Eu anomalies, REE distribution patterns, and Cr–Ni diagram, as well as the comparison with worldwide bauxite deposits, show that the ore-bearing rock series may have originated in the O–S mudrock, with contributions from the dolomite of the Gaopochang Formation. Furthermore, the position of the samples in the Al_2O_3–Fe_2O_3–SiO_2 ternary plot, the chemical index of alteration, and the strong positive correlations of some stable elements (such as Al, Ti, Zr, Hf, Nb, and Ta) indicates that the degree of weathering gradually increases from the O–S mudrock to the bauxitic mudrock, and further increases into the bauxite; the bauxitic mudrock and bauxite therefore originated from the O–S mudrock. The laterisation products of the O–S mudrock from the northern part of the ore collection area were transported to the karst depression in the early stages of the Middle Permian. The weathering products of the O–S mudrock and a small amount of the Gaopochang Formation dolomite accumulated on the karst interface, forming the original bauxite layers through cycles of compaction and concretion. These bauxite layers were then uplifted to or near the surface during the Late Cretaceous to Paleogene, eventually, forming karstic bauxite.

1. Introduction

Bauxite is a type of alluvial sedimentary ore related to weathering, and is rich in Al_2O_3 (generally >40%). The main chemical components in bauxite are Al, Fe, Si, and Ti (Bárdossy, 1989; Mordberg, 1996), and the principal mineral component is $Al(OH)_3$. Bauxite always forms in tropical and subtropical climates (Bogatyrev and Zhukov, 2009) and represents the raw material used to obtain Al and Ga (Calagari and Abedini, 2007; Ye et al., 2007; Bogatyrev and Zhukov, 2009; Liu et al., 2010). Depending on the petrology of the bedrock, bauxite is generally divided into two types, namely lateritic bauxite, hosted on silica-alumina rocks, and karstic bauxite, hosted on carbonate rocks (Mameli et al., 2007; Liu et al., 2010; Gu et al., 2013; Radusinović et al., 2017; Abedini et al., 2019).

Bauxite resources, which are distributed globally, are divided into 19 provinces, including the bauxite province of China (Bogatyev et al., 2009). The bauxite resources of Guizhou Province are abundant and distributed mainly in the northern, central, and south-eastern regions of

* Corresponding author.
E-mail address: xiaojiafei@vip.gyig.ac.cn (J. Xiao).

https://doi.org/10.1016/j.gexplo.2020.106676
Received 8 August 2019; Received in revised form 3 October 2020; Accepted 17 October 2020
Available online 20 October 2020

the province. The Kaili–Huangping bauxite-concentrated area in south-eastern Guizhou, which includes the Yudong bauxite deposit, is an important bauxite region (Dong, 2004; Fig. 1). Karstic bauxite in central and south-eastern Guizhou formed during the Early Carboniferous and Middle Permian, and overlies the unconformable Palaeozoic karst surface (Zhang et al., 2013a, 2013b; Long et al., 2017; Ling et al., 2018). The Yudong bauxite is of the karstic type, and the bedrock comprises dolomite of the Upper Devonian Gaopochang Formation.

Previous studies have focused on the characteristics of the ore-bearing rock series, including the geochemical characteristics, formation conditions, and the ore-controlling factors of the bauxite in the Kaili–Huangping bauxite-concentrated area, as well as the influence of the ancient karst landforms on bauxite formation (Dong, 2004; Li et al., 2012, 2013; Kong et al., 2013; Zhang et al., 2013a, 2013b; Liu et al., 2014). However, few detailed studies have been conducted on the geochemical characteristics of the bauxite deposits, the origins of the ore-forming material, and the metallogenic mechanism. In this study, the geochemical characteristics of the Yudong bauxite deposit and adjacent areas are investigated, and the Eh-pH conditions and parental affinity of the Yudong bauxite deposit are elucidated. Several deposits similar to the Yudong bauxite deposit exist in the Kaili–Huangping bauxite-concentrated area in south-eastern Guizhou, therefore this study of the formation conditions and parental affinity of the Yudong deposit will be beneficial for the exploration of this area.

2. Geological setting

Tectonically, the Kaili–Huangping bauxite-concentrated area forms part of the inner Yangtze landmass of the South China Block (Zhang et al., 2013a, 2013b; Fig. 1a). The Kaili–Huangping bauxite-concentrated area is located mainly in south-eastern Guizhou Province, China (Fig. 1b). Regionally, an EW-trending fault zone (consisting of the Huangping–Zhenyuan and Guiyang–Sansui Faults) occurs in central Guizhou (Fig. 1b) and is interpreted as a basement fracture (Guizhou Bureau of Geology and Mineral Resources, 1992). This fault zone and the NE-trending fault zone of eastern Guizhou (Fig. 1b) controlled the occurrence and development of the Palaeozoic sea–land distribution, uplift, and subsidence in the study area.

The Ziyun tectonic activity at the end of the Devonian resulted in the uplift of the study area, which lasted until the early Permian, resulting in the development of coastal plains (Guizhou Bureau of Geology and Mineral Resources, 1992). During this period, weathering and

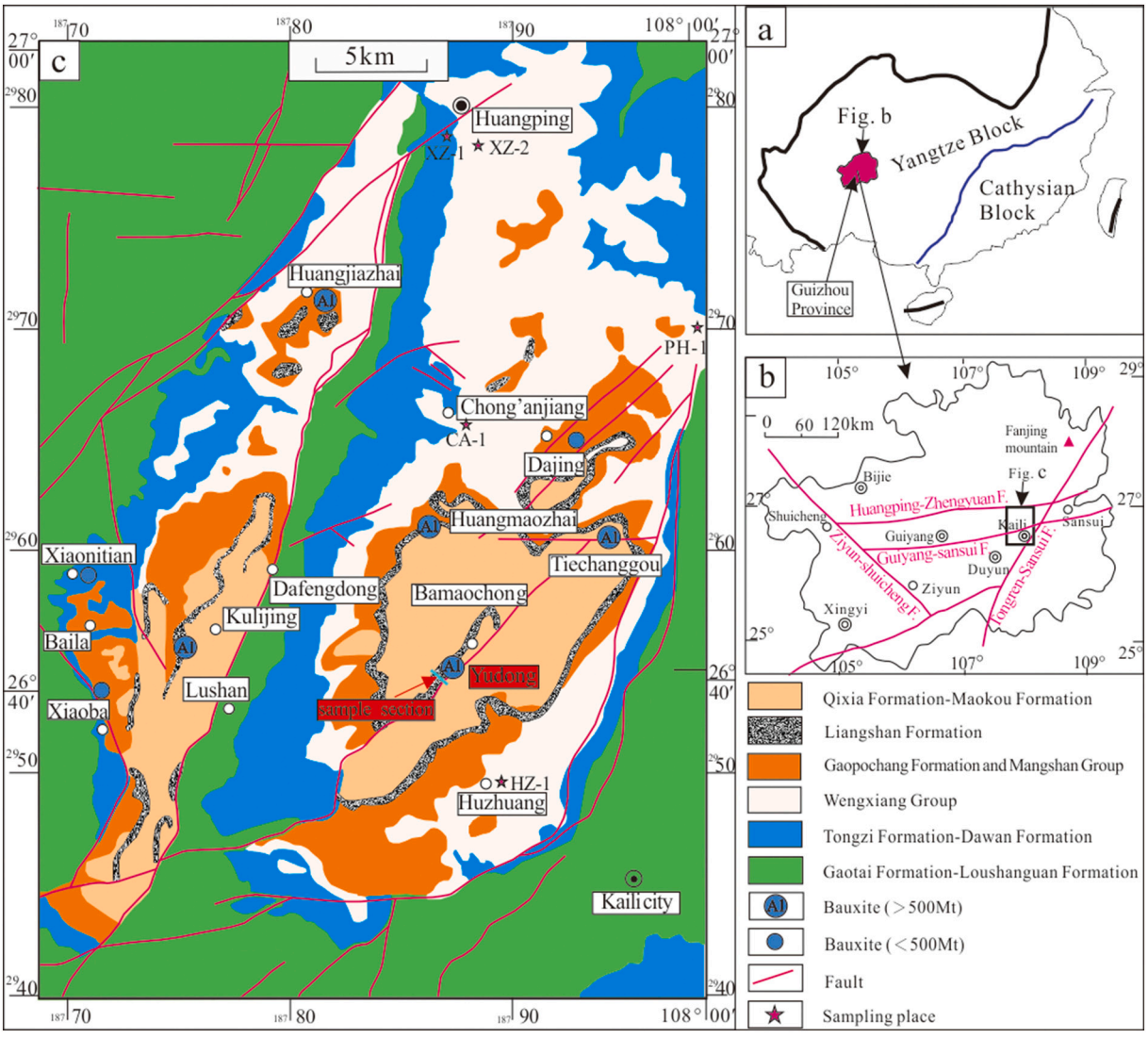

Fig. 1. Geological map illustrating geological features of bauxite deposits in northwestern Kaili, southeastern Guizhou Province, China. (a) Geotectonic location of Guizhou in South China Block (Zhang et al., 2013a, 2013b), (b) tectonic framework of Guizhou and the location of the study area (Guizhou Bureau of Geology and Mineral Resources, 1992), and (c) geological mining diagram of bauxite concentration area in Kaili (Guizhou Bureau of Geology and Mineral Resources, 1987; Zhang et al., 2013a, 2013b).

denudation produced an uneven karst interface on the Gaopochang Formation, which provided space for later bauxite deposition. Platform carbonate facies (the Jiusi, Shangsi, Baizuo, Huanglong, and Maping Formations) were deposited south of the Guiyang–Sansui fault after the early stages of the Early Carboniferous (Fig. 2; Guizhou Bureau of Geology and Mineral Resources, 1987). From the Devonian to the end of the Early Permian (Fig. 2), the area north of the Huangping–Zhenyuan Fault comprised land that likely consisted of piedmont plains and ultimately experienced long-term lateritic crustal weathering, providing sufficient source material for bauxite formation (Guizhou Bureau of Geology and Mineral Resources, 1987).

The regional strata and lithology comprise (Fig. 2, from early to late): dolomite of the Gaotai and Shilenshui Formations (of Cambrian Lower Miaolingian age) and Loushanguan Formation (of Cambrian Upper Miaolingian–Furongian age); dolomite of the Tongzi Formation, limestone of the Honghuayuan Formation, and mudstone of the Dawan Formation, all of which formed during the Lower Ordovician; mudstone and sandy shale of the Wengxiang Group (of Silurian Llandovery age); quartz sandstone and shale of the Mangshan Group (Middle and Lower Devonian age); dolomite of the Gaopochang Formation; mudstone and bauxitic rock of the Liangshan Formation and limestone of the Qixia and Maokou Formations, both of which are of Permian Guadalupian age; and modern Quaternary sediments, such as sand, gravel, clay, and fluvial alluvial sediments (Fig. 1c; Guizhou Bureau of Geology and Mineral Resources, 1987; Li et al., 2012; Zhang et al., 2012; Zhang et al., 2013a, 2013b). Most of the structures in the study area are NE-trending. In addition, the study area comprises three series of faults (NNE-, SN-, and NE-trending faults) and two folds, namely the Yudong and Dafengdong Synclines, with outcrops of the Liangshan Formation occurring along the two limbs (Fig. 1c; Zhang et al., 2012).

The Liangshan Formation can be divided into three members, from bottom to top: the lower member consists mainly of Fe-bearing bauxite mudrock; the middle member consists mainly of Al-bearing rock; and the upper member consists mainly of coal- or C-bearing mudrock. The lower member is composed of purple bauxitic mudrock with nodular siderite, with a thickness of 0–16 m. The middle member has a thickness of 0–40 m, and is composed of off-white bauxite with bauxitic mudrock. The types of bauxite ore in the middle member are clastic, pisolitic-oolitic, semi-earthy, earthy, and compact blocky bauxite. The upper member consists of brown–black poor coal, carbonaceous shale, and

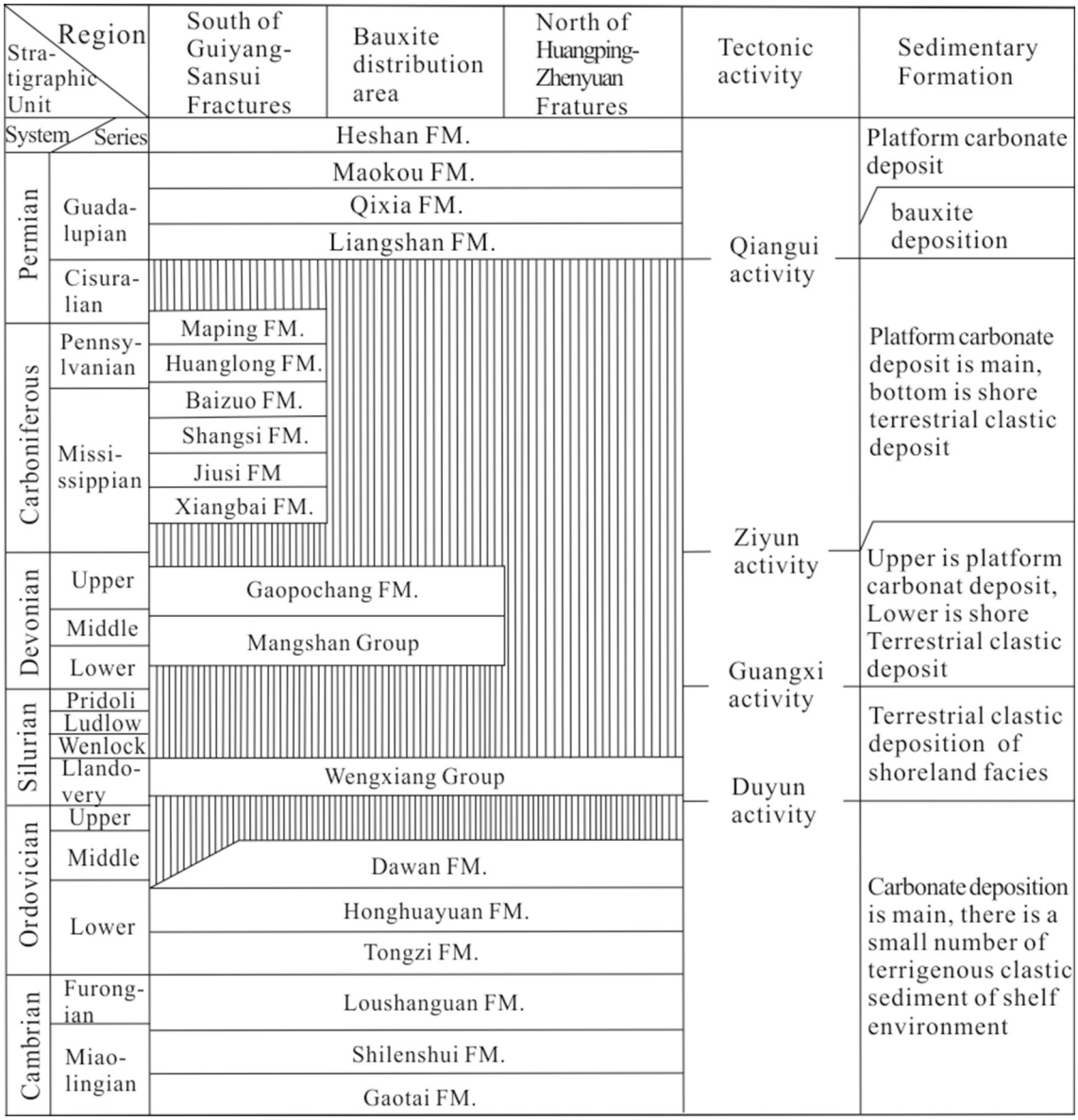

Fig. 2. Stratigraphic sequences of Yudong excavation and adjacent areas.

quartz sandstone, with a thickness of 1.2–13 m. The Fe-bearing and Al-bearing members both have variable thicknesses and are negatively correlated with each other (Li et al., 2012, 2013; Zhang et al., 2013a, 2013b), showing a length-wise transitional relationship.

3. Geological characteristics of the bauxite mining area

To date, several bauxite deposits have been discovered, including the Yudong, Huangjiazhai, Huangmaozhai, Tiechanggou, Xiaoba, and Kulijing deposits (Fig. 1c). The compositions of the ore-bearing rock series in these deposits and the underlying and overlying strata are similar; however, they differ in terms of thickness, mineralisation degree, and complete degree of the ore-bearing rock series. The axial direction of the Yudong Syncline in the study area is consistent with the NE-trending structures in the region. The ore-hosting strata are distributed along, and limited by, the two limbs of the Yudong Syncline (Fig. 1c). The ore-bearing rock series of the Yudong bauxite controlled the spatial distribution and longitudinal changes in the bauxite deposits. The ore-bearing rock series (Figs. 3a and 4) is composed of an Fe-bearing member (Fig. 3b–d) and an Al-bearing member (Fig. 3e and f).

The sampling site for the Yudong bauxite is located approximately 2 km SW of Yudong village. At this site, the Fe-bearing member is composed of purple Fe-bearing bauxitic mudrock with a thickness of 3.5 m. The Al-bearing member is composed of off-white earthy (Fig. 3g), half-earthy (Fig. 3h), and compact blocky (Fig. 3i) bauxite, along with purple and off-white bauxitic mudrock, with a thickness of approximately 5 m (Figs. 3a and 4). The breadth of the ore-bearing rock series ranges from 10 cm to 2 m. Many lenses of the ore-bearing rock series have been discovered, and thicker ore beds are distributed in the lenses. The overlying coal-bearing (carbonaceous) member is composed of black shale, poor coal, and sandstone, with a thickness of 13 m (Figs. 3a and 4).

Scanning electron microscopy (SEM) and X-ray diffraction (XRD) analysis show that the ore mineral in the Yudong bauxite mainly consists of unordered diaspore (Figs. 5a–c and 6), along with some boehmite (Fig. 5d). The diaspore textures include columnar, acicular, and prismatic varieties. The Yudong bauxite also contains clay minerals, including kaolinite and chlorite, and heavy minerals, including anatase, rutile, and zircon (Figs. 5 and 6).

4. Geochemical characteristics

Twenty samples were collected consecutively from a cross-sectional profile through the Yudong ore area, and five samples were collected from the underlying ancient strata of the peripheral area (Fig. 1c). The latter were denoted as O–S (Ordovician–Silurian) mudrock, and consist of the Dawan Formation (Ordovician) and the Wengxiang Group (Silurian). Major elements were analysed using an Axios (PW4400) X-ray fluorescence instrument at the State Key Laboratory of Ore Deposit Geochemistry, Institute of Geochemistry, Chinese Academy of Sciences. A solution containing 0.7 g of sample and 7 g of solvent was completely digested using 1 ml $LiNO_3$ and 0.5 ml LiBr in a Pt crucible, then melted at 1150 °C for 20 min. The solution was poured into a meld and to prepare a glass disk for analysis. The methodology used for the chemical analysis

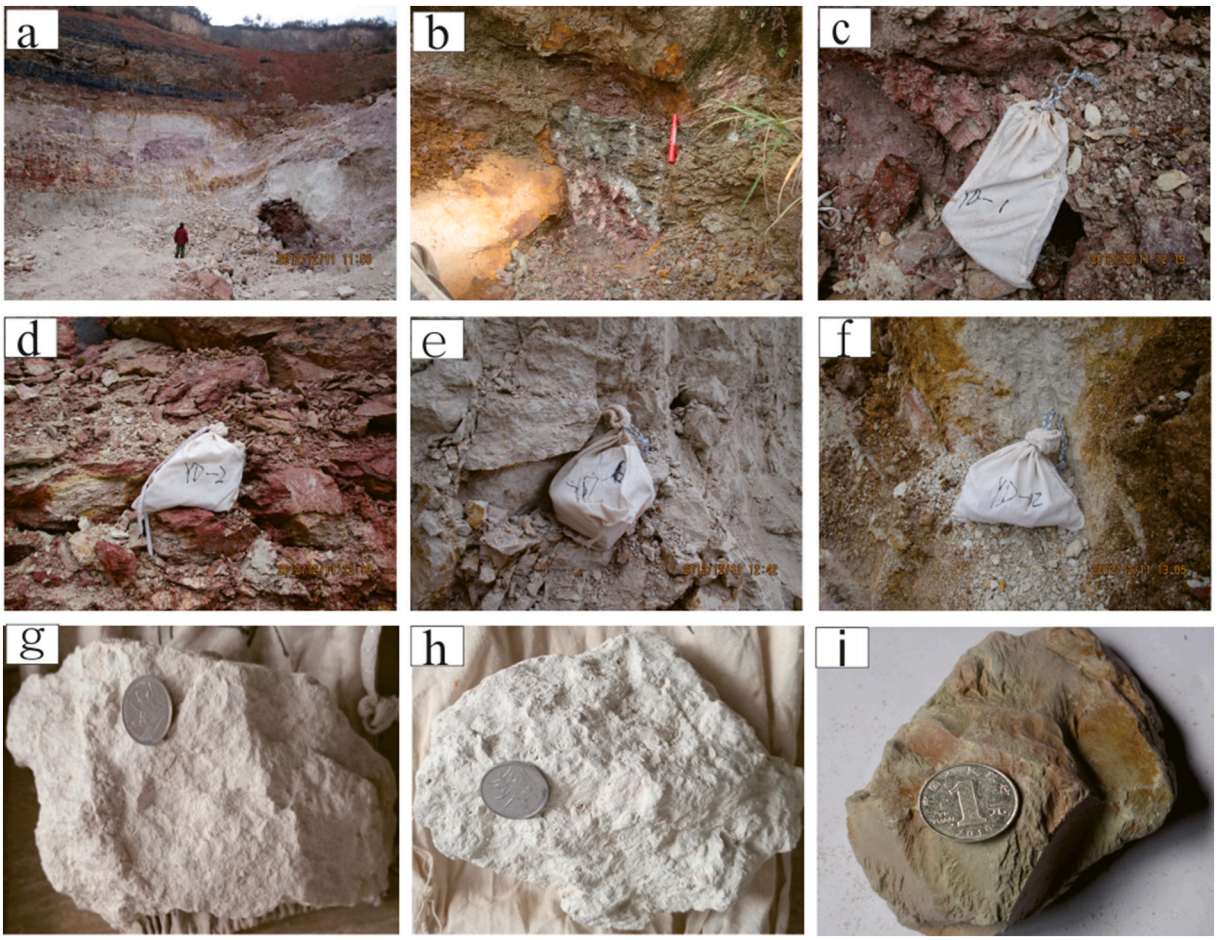

Fig. 3. Profile outcrops and ore types in Yudong bauxite excavation. (a) General image of profile, (b) outcrop of lower Fe-bearing member, (c) outcrop of middle Fe-bearing member, (d) outcrop of upper Fe-bearing member, (e) outcrop of middle Al-bearing member, (f) outcrop of top Al-bearing member, (g) sample of earthy bauxite, (h) sample of half-earthy bauxite, and (i) sample of compact blocky bauxite.

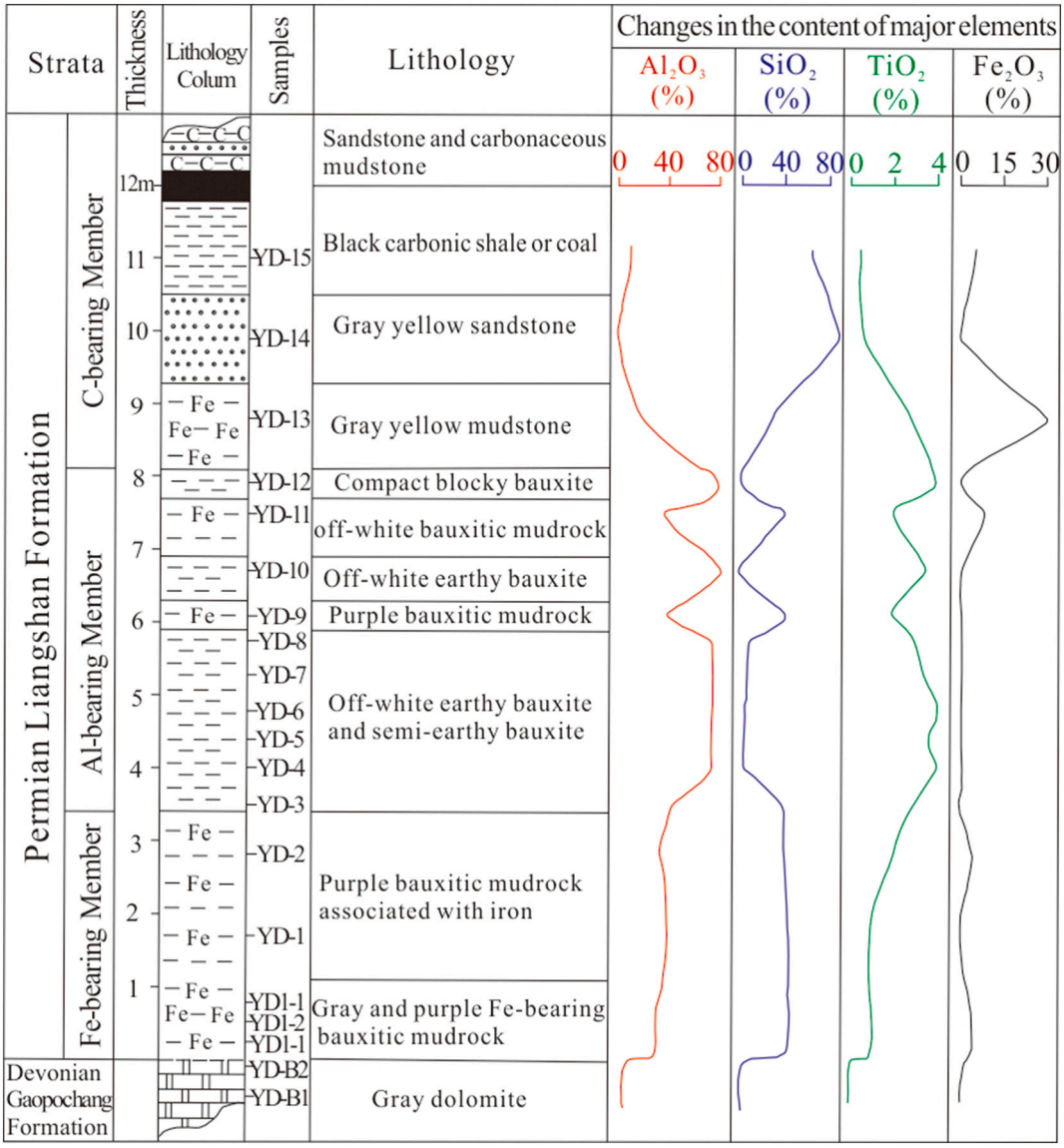

Fig. 4. Stratigraphic column and variations in Al_2O_3, SiO_2, Fe_2O_3, and TiO_2 in profile of Yudong bauxite deposits.

of the aluminium ores via the determination of element contents using the X-ray fluorescence spectrometric method is based on the non-ferrous metal industry standard of the People's Republic of China (YS/T 575. 23-2009). The error in the results was <5%. Trace elements were analysed using a quadrupole inductively coupled plasma mass spectrometer (ELAN-DRC-e ICP-MS) at the State Key Laboratory of Ore Deposit Geochemistry. A solution of 1 ml HF and 1 ml HNO_3 was used to completely digest 50 mg of each sample. The internal standard was a 40 ng/ml Rh solution, and the methods described by Qi et al. (2000) were followed. International standard samples (AGV-2, AMH-1, and GBPG-1) were used and the error in the results was <5%. The analytical results are shown in Table 1.

4.1. Major elements

As shown in Table 1, the major elements of the ore-bearing rock series are Al, Si, Fe, and Ti, and smaller amounts of other elements are also present. The Al_2O_3, SiO_2, Fe_2O_3, and TiO_2 contents of the off-white bauxites (eight samples) in the Al-bearing member are 44.21–80.81%, 0.45–38%, 0.79–1.34%, and 2.84–4.24%, respectively. The Al_2O_3, SiO_2, Fe_2O_3, and TiO_2 contents of the purple bauxitic mudrock (two samples) in the Al-bearing member are 36.52–42.31%, 39.02–41.6%, 0.62–9.07%, and 1.96–3.92%, respectively. The Fe content of the overlying grey–yellow mudrock is high (29.65%), and this unit grades into Fe-bearing oolitic mudrock laterally. The Al_2O_3 content of the grey–yellow mudrock decreases sharply to 20.34%.

The bauxite in the Al-bearing member contains more Al and Ti, and less Si and Fe, than the purple and grey–yellow mudrocks. The Al_2O_3, SiO_2, Fe_2O_3, and TiO_2 contents of the purple bauxitic mudrock in the Fe-bearing member are 32.93–39.49%, 41.92–45%, 0.64–5.09%, and 0.96–2.05%, respectively. Fig. 4 shows the variations in the contents of some of the major elements in the ore-bearing rock series of the Yudong bauxite, to illustrate the relationships between these compounds in the sampled profile. Al_2O_3 is positively correlated with TiO_2, negatively correlated with SiO_2, and not correlated with Fe_2O_3. TiO_2 is negatively correlated with SiO_2 and not correlated with Fe_2O_3. SiO_2 is not correlated with Fe_2O_3. These relationships are consistent with those shown in the scatter plots in Fig. 7, and indicate that bauxite formed via an Fe- and Si-leaching and Al-enrichment process. In terms of the chemical composition of the O–S mudrock on the periphery of the bauxite mining area, the five samples have Al_2O_3, SiO_2, Fe_2O_3, and TiO_2 contents of 15.04–17.28%, 60.13–67.58%, 5.08–7.22%, and 0.62–0.76%,

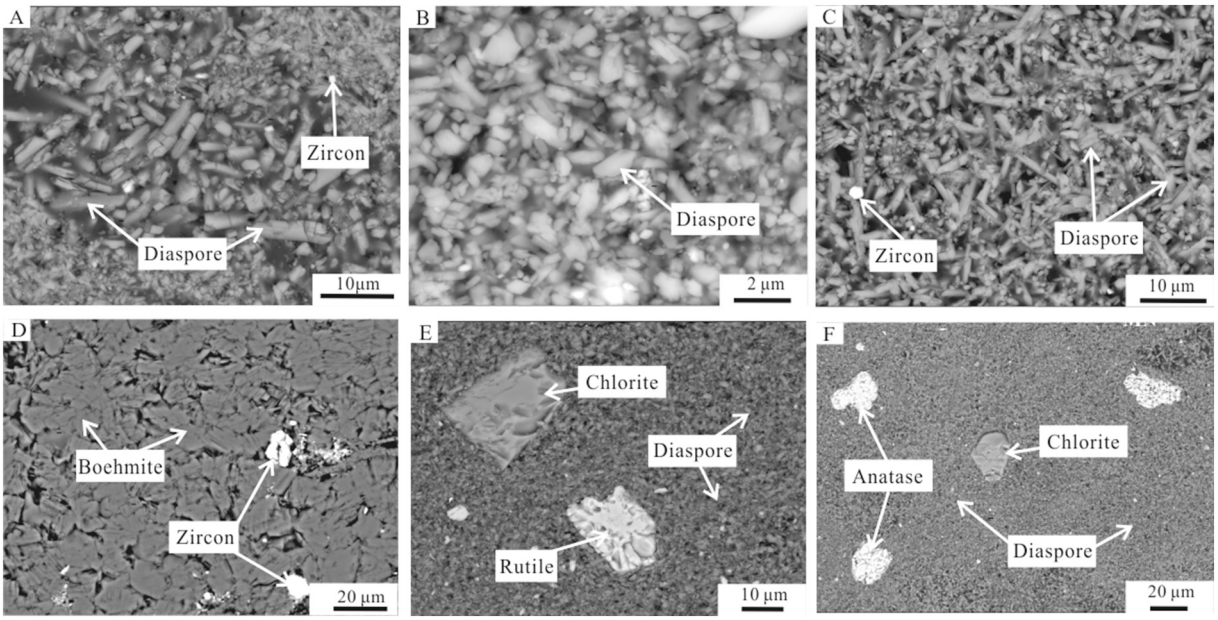

Fig. 5. SEM image of some minerals in Yudong bauxite: (a)–(c) diaspore and zircon, (d) boehmite and zircon, (e) chlorite and rutile, (d) chlorite and anatase.

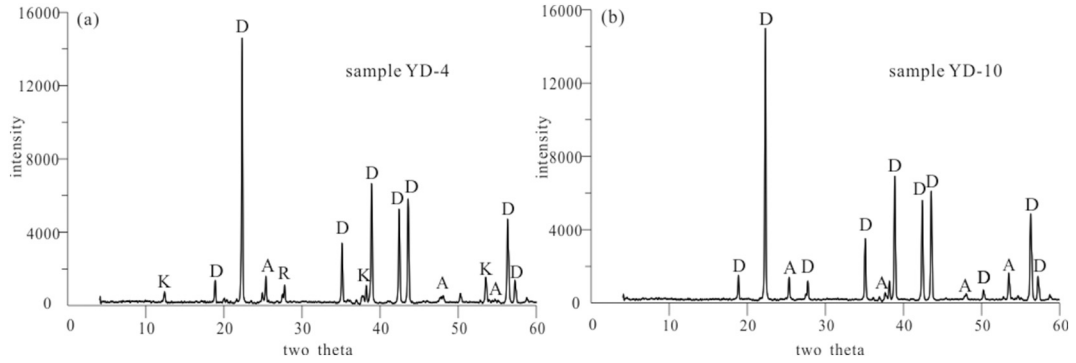

Fig. 6. The XRD patterns for two typical analysed samples from Yudong bauxite (D: diaspore, A: anatase, K: kaolinite, R: rutile).

respectively.

Ternary plots of Al_2O_3, Fe_2O_3, and SiO_2 are typically used to indicate weathering trends. According to these plots (Fig. 8; Schellmann, 1986), the Yudong bauxite samples occur in a strong laterisation zone, and the purple Fe-bearing mudrock lies in a transition zone from weak to moderate laterisation. The O–S mudrock occurs in a kaolinisation zone, indicating that this lithology underwent weak alteration. The chemical index of alteration (CIA) can also indicate the degree of rock weathering (Nesbitt and Young, 1982; Radusinović et al., 2017). The CIA of the O–S mudrock is low (75; Table 1), whereas that of the Fe-bearing member is much higher (87–99), and that of the Al-bearing member indicates the highest degree of weathering (99). Thus, the degree of weathering based on the CIA is consistent with the interpretations from the ternary plots.

In the sample correlation diagrams (Fig. 7), Al_2O_3 is positively correlated with TiO_2 (with an R^2 of 0.92; Fig. 7a), and Al_2O_3 and TiO_2 are negatively correlated with SiO_2 (with an R^2 of 0.98 and 0.89, respectively; Fig. 7b and c). Al_2O_3 and Fe_2O_3 in the O–S mudrock are positively correlated, whereas Al_2O_3 and Fe_2O_3 in the bauxite samples show no correlation (Fig. 7d). This indicates that Fe remained stable during the initial weathering stage of the O–S mudrock, but became unstable after weathering and during percolation characterised by strong laterisation. TiO_2 and SiO_2 show no correlation with Fe_2O_3 (Fig. 7e and f). The correlations between the main oxides (K_2O, Na_2O, CaO, P_2O_5, MgO, and MnO) and Al_2O_3 indicate that these elements migrated, and became depleted with increasing Al_2O_3 content (Table 1). Al_2O_3 shows a strong positive correlation with TiO_2, and the correlation line passes through the O–S mudrock sample composition. The positive correlation indicates relationships between the bauxite, bauxitic mudrock, and O–S mudrock, which are consistent with the residual enrichment of Ti and Al in the strongly weathered profiles. The positions of the sample compositions in the Al_2O_3–Fe_2O_3–SiO_2 ternary plot, the CIA, and the strong positive correlations of some stable elements (such as Al, Ti, Zr, Hf, Nb, and Ta) indicate that the degree of weathering increases gradually from the O–S mudrock, to the bauxitic mudrock, and further increases into the bauxite. The bauxitic mudrock and bauxite therefore originated from the O–S mudrock.

4.2. Trace elements

Some trace elements, such as V, Cr, Zr, Nb, Hf, Ta, Th, and U, are more abundant in the Fe- and Al-bearing members than in the O–S mudrock (Table 1). In addition, these elements are more abundant in the Al-bearing than in the Fe-bearing member, and the contents of these elements increase with increasing degree of weathering.

The North American shale composite (NASC; Gromet et al., 1984) normalised trace element distributions (Fig. 9) reveal that the NASC-normalised contents of the O–S mudrock samples fluctuate approximately around 1. The trace elements in the Fe-bearing member change

Table 1
Chemical composition of representative samples from the Yudong bauxite deposit, Kaili-Huangping area.

	XZ-1	XZ-2	CA-1	HZ-1	PH-1	YD-B1	YD1-1	YD1-3	YD-1	YD-2	YD-3	YD-4	YD-5	YD-6	YD-7	YD-8	YD-9	YD-10	YD-11	YD-12	YD-13
Al_2O_3 (%)	15.60	17.28	16.40	15.04	16.82	0.21	32.99	34.01	39.49	37.42	44.21	76.07	75.01	75.37	75.77	73.53	42.31	80.81	36.52	80.13	20.34
Fe_2O_3	5.65	6.77	6.15	5.08	7.22	0.38	5.09	3.91	0.64	4.90	0.86	1.34	0.91	0.85	0.85	0.87	0.62	0.79	9.07	0.80	29.65
SiO_2	64.47	61.33	60.37	67.58	60.13	1.08	43.81	44.77	45.00	41.92	38.10	3.47	5.75	3.55	5.54	7.57	41.60	0.45	39.02	0.54	32.18
TiO_2	0.70	0.69	0.73	0.62	0.76	0.02	1.25	1.20	0.96	2.05	2.84	4.24	3.63	4.19	3.37	3.09	1.99	3.47	2.17	3.92	2.82
MgO	2.72	2.90	2.88	2.38	3.04	20.53	1.82	1.54	0.20	0.10	0.08	0.07	0.05	0.08	0.04	0.05	0.06	0.04	0.09	0.05	0.81
CaO	1.26	1.10	2.60	0.61	1.52	32.47	0.42	0.24	0.12	0.09	0.07	0.08	0.43	0.06	0.07	0.06	0.10	0.06	0.09	0.07	0.35
Na_2O	0.59	0.71	0.71	0.53	0.79	–	0.09	0.08	0.04	0.04	0.02	0.26	0.02	0.02	0.02	0.03	0.03	0.02	0.02	0.03	0.07
K_2O	4.08	4.44	4.09	4.18	4.05	0.04	3.85	3.55	0.81	0.05	0.05	0.04	0.01	0.00	0.00	0.00	0.04	0.01	0.03	0.01	2.28
P_2O_5	0.15	0.12	0.13	0.17	0.14	–	0.11	0.10	0.06	0.18	0.19	0.16	0.23	0.21	0.23	0.21	0.11	0.23	0.16	0.24	0.11
MnO	0.06	0.08	0.06	0.04	0.06	0.01	0.02	0.02	0.01	0.00	0.00	0.01	0.00	0.00	0.00	0.00	0.00	0.00	0.00	0.00	0.02
LOI	4.60	4.57	5.66	3.75	5.10	45.56	10.10	10.44	13.57	13.63	13.55	14.49	14.05	14.45	14.59	14.56	13.51	14.55	13.09	14.52	12.01
Total	99.9	100.1	99.9	100.1	99.7	100.3	99.6	99.9	100.9	100.4	99.9	100.2	100.1	98.78	100.5	99.96	100.4	100.4	100.3	100.3	100.6
Sc (ppm)	12.2	15	14.7	11.6	14.4	–	10.9	9.51	13.5	17.1	12.4	11.8	11.2	13.4	12.1	10.4	8.63	9.44	25.7	9.51	29.9
V	97.4	117	113	85.8	110	7.3	304	200	142	197	191	285	444	363	506	570	150	660	294	726	675
Cr	74.9	87.7	86.3	69.2	82	–	158	133	83.2	200	202	178	217	211	229	198	123	220	221	229	244
Co	13.5	17.3	16.8	14.4	17.2	6.03	19.8	18.9	2.77	6.85	5.13	2.71	2.34	2	5.41	1.39	4.08	2.51	4.04	1.93	2.02
Ni	37.7	46	44.6	36	44	10	155	133	49.16	52.79	32.78	5.73	6.39	5.72	7.41	6.69	34.10	3.63	31.53	1.71	6.61
Ga	20.6	22.7	21.7	19.1	21.3	0.34	35.7	32.1	20.2	29.5	29.6	37	44.6	40.9	43	44.9	16.40	37.80	35.2	35	64.2
Sr	63.2	74.6	90.9	58.5	77.9	93.4	233	198	66.5	160	142	67.5	44.6	62.7	65.2	39.1	167	64.5	85.4	87.2	143
Y	25.7	23.5	28.3	18.7	26.7	1.43	40.3	40.6	9.66	26.9	25	27.4	25.6	32.8	23.9	24.5	11.9	24.2	36.1	22.9	65.6
Zr	199	166	156	128	142	2.83	294	292	211	1140	1720	2090	1860	2290	1720	1390	604	1800	1370	2260	1000
Nb	15.95	16.48	17.84	11.26	17.31	0.28	31.59	31.90	22.89	41.22	55.94	78.66	72.89	83.73	68.59	65.32	40.79	69.79	46.21	77.97	58.86
Cs	10.79	12.01	11.68	10.25	11.90	0.10	13.22	12.34	4.92	0.24	0.23	0.05	0.04	0.03	0.04	0.04	0.20	0.05	0.21	0.04	18.8
Ba	380	574	797	529	566	4.81	277	259	78.6	8.85	9.22	4.48	2.9	3.89	3.21	2.17	6.37	3.89	8.37	4.85	309
Hf	5.94	4.77	4.53	3.70	4.34	0.04	9.38	9.31	5.76	40.8	54.2	63.3	58.6	72.5	55	50.6	18.8	53.4	48	67.3	31.9
Ta	1.26	1.24	1.40	0.90	1.35	0.12	2.55	2.64	1.70	3.12	4.21	5.60	5.40	6.00	5.38	5.15	3.11	5.62	3.76	6.43	4.78
Th	17.4	18.2	19.5	16.6	19	0.19	33.7	35.4	14.1	38.5	30.7	34	37.7	38.5	39.2	32.5	17.9	39.7	49.9	43.4	63.7
U	3.52	3.36	4.12	2.88	3.03	0.24	9.75	10	5.3	6.94	8.99	18.5	14.5	16	13.6	12.8	5.59	13.9	7.83	13.5	14.3
La	45.4	46.2	46.2	41.4	45.3	0.89	107	103	19.1	11.7	25.6	10.8	6.01	9.77	7.89	5.61	28	7.34	18.3	23.4	135
Ce	87.8	86.4	89.5	80.4	86.5	1.84	199	192	45.7	25.2	53	21.1	13	18.6	17.9	13.3	58.6	20.1	42.2	54	253
Pr	9.41	9.17	9.9	8.84	9.82	0.20	25	23.1	2.5	2.74	3.87	1.69	1.03	1.5	1.46	0.98	3.97	1.65	3.52	4.53	22.2
Nd	34.4	32.9	36.7	32.4	36.4	0.74	92.7	85.6	7.06	10.7	12.2	6.62	4.22	5.70	5.97	3.93	13.1	6.25	13	16.5	60.9
Sm	5.79	5.22	6.65	5.59	6.8	0.15	14	12.8	1.22	2.29	2.4	1.82	1.2	1.76	1.65	1.30	2.59	1.47	3.02	3.1	8.82
Eu	1.12	0.94	1.21	1.01	1.24	0.03	2.12	1.89	0.22	0.53	0.54	0.47	0.33	0.45	0.41	0.36	0.49	0.38	0.66	0.56	1.65
Gd	5.24	4.29	5.71	4.57	5.84	0.13	8.83	8.71	1.35	2.70	2.57	2.52	1.97	2.63	2.21	2.52	1.81	2.25	3.31	2.71	9.27
Tb	0.81	0.73	0.90	0.68	0.91	0.02	1.34	1.27	0.24	0.62	0.56	0.57	0.52	0.72	0.52	0.59	0.33	0.53	0.81	0.54	1.84
Dy	4.52	3.97	5.21	3.5	4.9	0.16	6.68	6.72	1.6	4.13	3.77	4.4	3.84	4.99	3.87	4.1	2.13	3.80	5.74	3.96	12.2
Ho	0.892	0.823	1.01	0.687	0.964	0.03	1.43	1.4	0.40	0.98	0.97	1.06	1.01	1.22	0.91	0.91	0.47	0.95	1.41	0.93	2.67
Er	2.59	2.55	2.9	2.04	2.93	0.09	4.54	4.53	1.14	3.18	3.12	3.43	3.17	3.89	3.03	3.1	1.53	3.1	4.62	2.95	8.61
Tm	0.39	0.36	0.43	0.30	0.40	0.01	0.68	0.65	0.22	0.51	0.48	0.54	0.50	0.61	0.46	0.49	0.25	0.51	0.8	0.46	1.39
Yb	2.44	2.57	2.72	1.9	2.55	0.07	4.67	4.36	1.48	4.04	3.91	4.37	4.06	4.76	3.8	3.54	1.9	3.76	5.8	3.82	9.64
Lu	0.34	0.37	0.40	0.28	0.38	0.01	0.69	0.69	0.21	0.61	0.61	0.65	0.55	0.65	0.55	0.51	0.31	0.55	0.91	0.55	1.49
∑REE	201.16	196.49	209.43	183.60	204.94	4.35	468.67	446.72	82.44	69.92	113.59	60.05	41.41	57.24	50.63	41.23	115.47	52.64	104.11	118.00	528.68
∑L/∑H	10.67	11.55	9.87	12.15	9.86	7.50	15.24	14.77	11.43	3.17	6.11	2.42	1.65	1.94	2.30	1.62	12.24	2.41	3.45	6.42	10.22
Ce/Ce*	1.02	1.01	1.01	1.01	0.99	1.06	0.93	0.95	1.59	1.07	1.28	1.19	1.26	1.17	1.27	1.37	1.34	1.39	1.27	1.26	1.11
Eu/Eu*	0.62	0.61	0.60	0.61	0.60	0.63	0.58	0.55	0.53	0.65	0.66	0.67	0.66	0.64	0.66	0.62	0.69	0.64	0.64	0.59	0.56
La/Y	1.77	1.97	1.63	2.21	1.70	0.63	2.66	2.54	1.98	0.43	1.02	0.39	0.23	0.30	0.33	0.23	2.35	0.30	0.51	1.02	2.06
(La/Yb)N	7.49	8.71	7.89	12.54	12.12	14.63	15.45	15.93	8.70	1.95	4.41	1.67	1.00	1.38	1.40	1.07	9.94	1.32	2.13	4.13	9.44
CIA	72.46	73.44	68.91	73.87	72.56	–	88.33	89.78	97.60	99.54	99.69	99.51	99.40	99.89	99.88	99.87	99.62	99.88	99.62	99.87	88.28

$Eu/Eu^* = [Eu_n/(Sm_n \cdot Gd_n)^{1/2}]$; $Ce/Ce^* = [Ce_n/(La_n \cdot Pr_n)^{1/2}]$; chondrite values are from Boynton (1984).

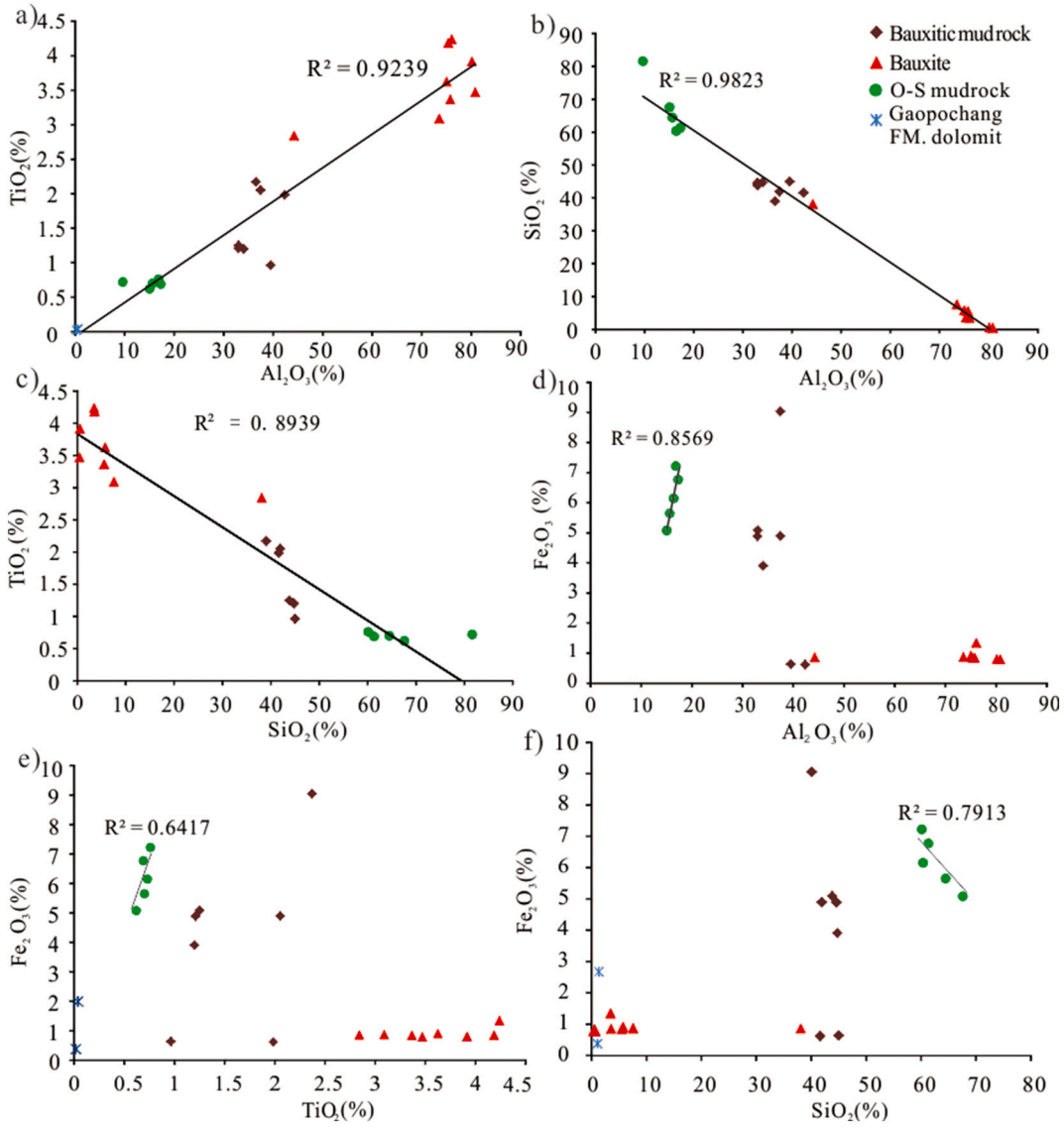

Fig. 7. Scatter plots of (a) TiO_2 vs. Al_2O_3, (b) SiO_2 vs. Al_2O_3, (c) TiO_2 vs. SiO_2, (d) Fe_2O_3 vs. Al_2O_3, (e) Fe_2O_3 vs. TiO_2, and (f) Fe_2O_3 vs. SiO_2 of ore-bearing rock series in Yudong profile, together with Ordovician–Silurian (O–S) mudrock.

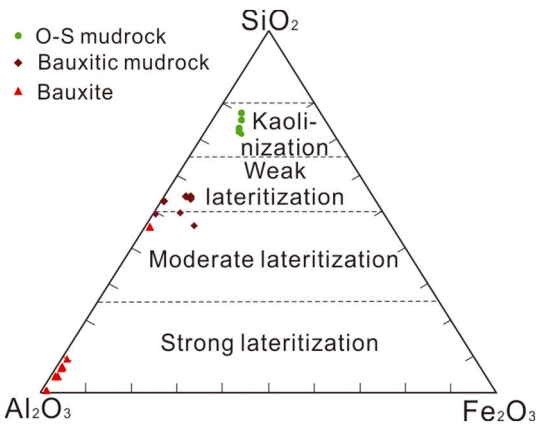

Fig. 8. SiO_2–Al_2O_3–Fe_2O_3 ternary plot for ore-bearing rock series in Yudong profile, together with the O–S mudrock (Schellmann, 1986).

gradually from the lower to the upper part. The contents in the lower part are close to those of the NASC, whereas those in the middle part vary slightly, and those in the upper part increase appreciably, revealing a transition to bauxite. The changes in the trace element contents of the Al-bearing member profile are very similar. Generally, the Sc and Y contents are close to that of the O–S mudrock samples, whereas the Co, Ni, Cs, and Ba contents are lower, and the Zr, Nb, Hf, Ta, Th, and U contents are higher. The Sc, V, Cr, and Y contents of the overlying grey–yellow mudrock are higher than those of the bauxite. The Sr content is close to that of NASC, whereas the Co and Ni contents are lower, and the Zr, Nb, Cs, Hf, Ta, Th, and U contents are higher.

In summary, the elemental differences between the Fe-bearing and Al-bearing members reflect the bauxitisation process. During this process, some elements were stable (such as Sc and Y), some were depleted (such as Cs and Ba), and others were enriched (such as V, Zr, Nb, Hf, Ta, Th, and U). Correlation analyses indicate that TiO_2 and Al_2O_3 are positively correlated with high-field-strength elements, including Zr, Nb, Hf, and Ta (Fig. 10a–d). Furthermore, Zr is positively correlated with Hf, Ta, and Nb, and Ta is positively correlated with Nb. The correlation coefficients (R^2) are 0.99 for Zr–Hf, 0.91 for Zr–Ta, 0.93 for Zr–Nb, and 0.99 for Ta–Nb (Fig. 11a–d). These correlations indicate that

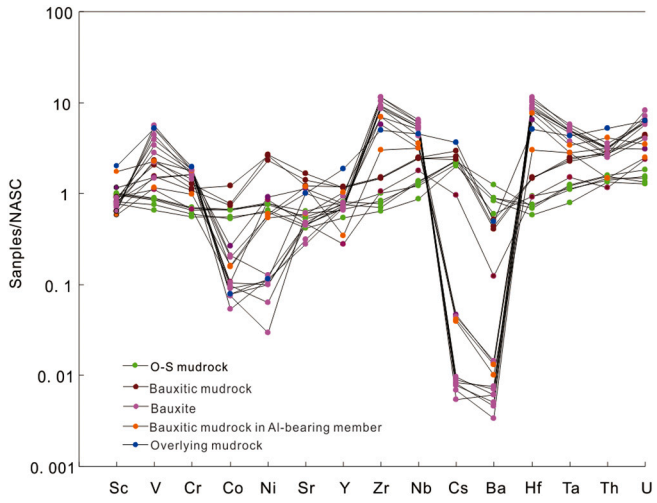

Fig. 9. North American shale composite (NASC)-normalised (Groment et al., 1984) trace element distributions of ore-bearing rock series Yudong profile and O–S mudrock.

the high-field-strength elements were gradually enriched during bauxite mineralisation.

4.3. Rare earth elements

The rare earth element (REE) contents of the samples from the Yudong profile and the peripheral O–S mudrock are given in Table 1. The chondrite-normalised (Boynton, 1984) REE distributions of all samples are shown in Fig. 12. As shown in Table 1, the total REE content, ΣREE, of the purple bauxitic mudrock at the bottom of the Fe-bearing member ranges from 372.56 to 468.67 ppm, whereas ΣREE decreases abruptly in the middle section to approximately 80 ppm, and further decreases in the upper section to approximately 70 ppm. The ΣREE of the Al-bearing bauxite member is low, ranging from 41.41 to 117.99 ppm, while the ΣREE of the purple bauxitic mudrock interlayer is in the range 104–115 ppm, and that of the overlying grey–yellow mudrock reaches 528.68 ppm. The ΣREE of the Gaopochang Formation dolomite is very low, approximately 5 ppm, whereas that of the O–S mudrock ranges from 183.6 to 209.43 ppm.

Regarding the chondrite-normalised (Boynton, 1984) REE distributions of the ore-bearing rock series, O–S mudrock, Gaopochang Formation dolomite and overlying grey-yellow mudrock (Fig. 12), in general, the LREEs of all samples show a right-leaning distribution, whereas, the HREEs had difference distribution. In the lower part of the Fe-bearing member, O–S mudrock and Gaopochang Formation dolomite, the HREEs show right-leaning distribution; In the middle-upper part of the Fe-bearing member, the Al-bearing member and the overlying grey-yellow mudrock, the HREEs exhibit a left-leaning distribution.

In conclusion, the ΣREE curves of the sampled profile show distinct changed plots (Fig. 13a). The ΣREE of the overlying grey–yellow mudrock is the highest at 530 ppm, whereas the ΣREE of the purple bauxitic mudrock in the lower part of the Fe-bearing member shows a peak at 400 ppm. In the middle to upper parts of the Fe- and Al-bearing members, ΣREE is typically <100 ppm. The Gaopochang Formation dolomite shows the lowest ΣREE (4–10 ppm). The ΣREE of the O–S mudrock is approximately 200 ppm. The ΣREE values increase systematically from the Al-bearing to the Fe-bearing member across the sampled profile, and the REEs show fractionation. The $(La/Yb)_N$ value varies markedly, from 1 to 15.9, and increases downwards, similarly to the REE characteristics of the bauxite of the Wuchuan–Zheng'an–Daozhen area, in northern Guizhou (Wang et al., 2013).

The δCe distribution curves of the sampled profile (Table 1, Fig. 13b) show that the δCe values of the Gaopochang Formation dolomite are slightly higher than 1, whereas those of the Al-bearing member range from 1.2 to 1.4. The δCe values of the lower part of the Fe-bearing member are <1, whereas those in the middle to upper parts change appreciably, increasing to 1.6 in the middle and decreasing to 1.1 in the upper part. In contrast, the δCe values of the O–S mudrock show no anomalies. The δEu value changes slightly along the profile (Table 1, Fig. 13c). The δEu value of the Gaopochang Formation dolomite is in the

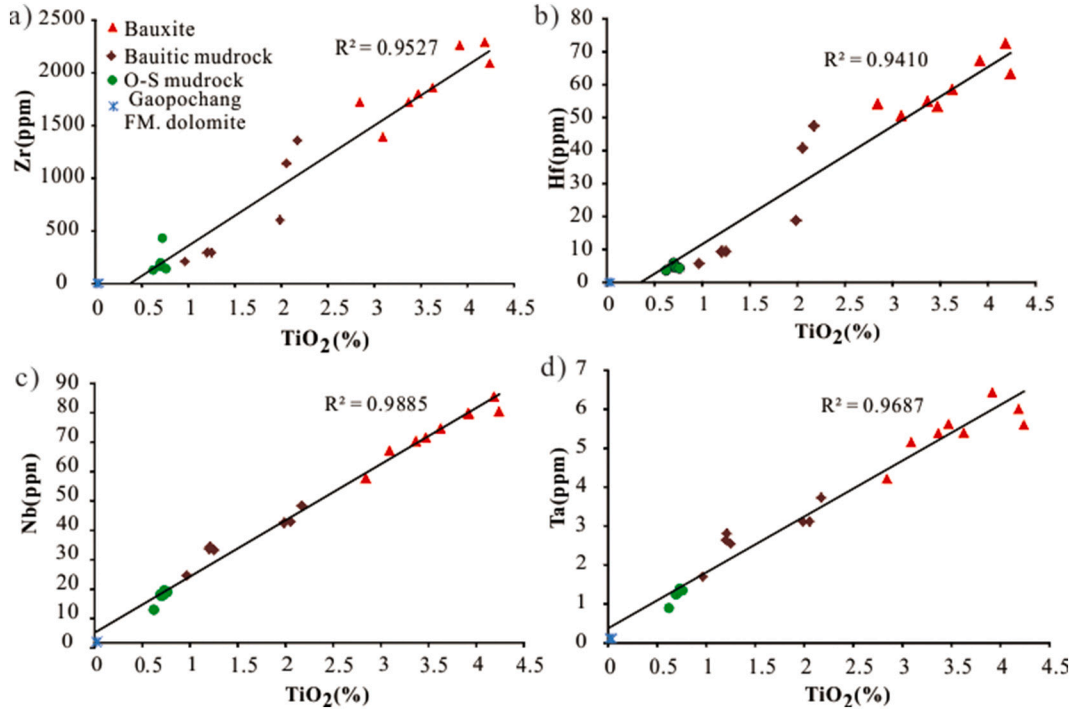

Fig. 10. Binary diagrams for selected trace elements showing correlations between (a) Zr, (b) Hf, (c) Nb, and (d) Ta with TiO_2 in ore-bearing rock series of Yudong profile and O–S mudrock.

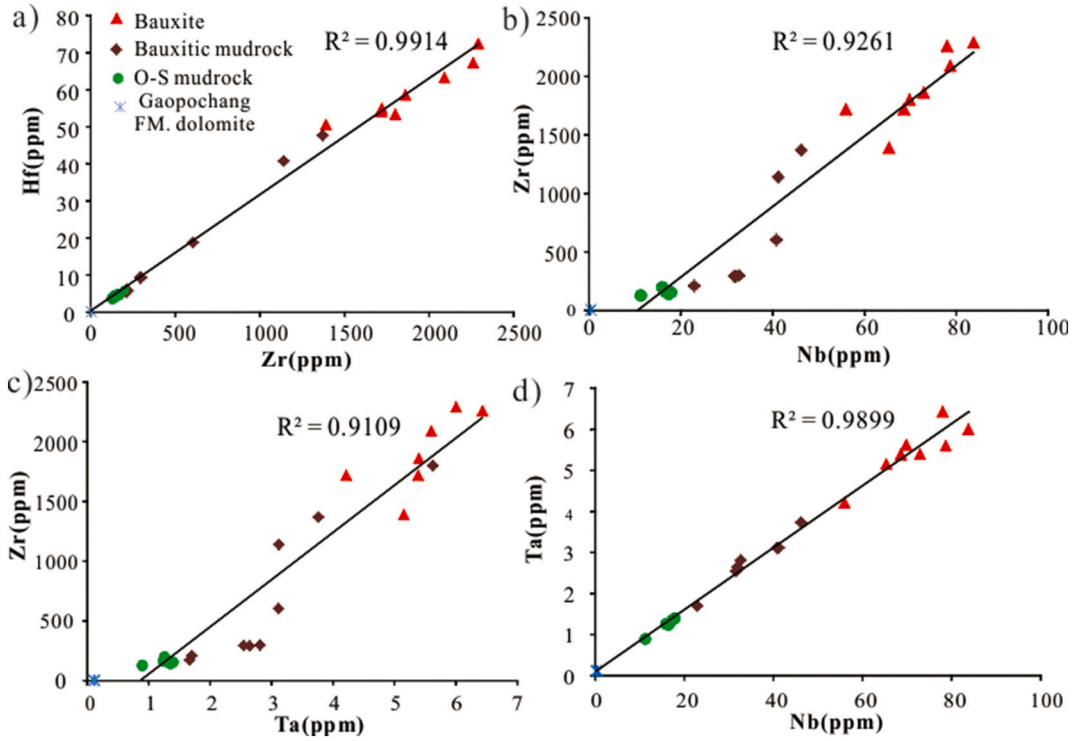

Fig. 11. Correlation graphs of (a) Zr and Hf, (b) Zr and Nb, (c) Zr and Ta, and (d) Nb and Ta.

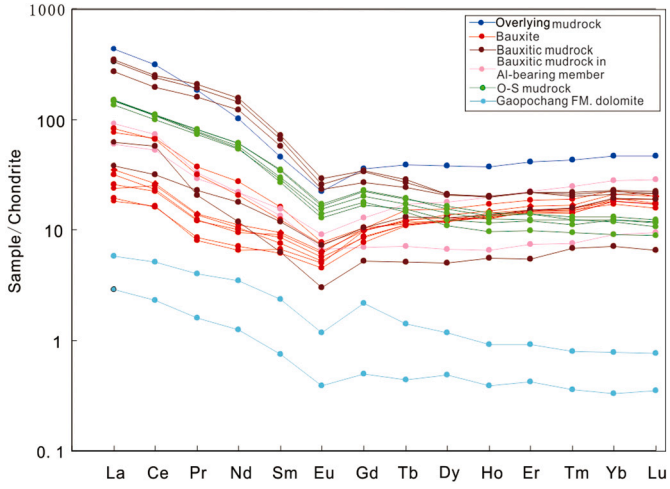

Fig. 12. Chondrite-normalised (Boynton, 1984) rare earth element (REE) distributions of ore-bearing rock series in Yudong profile and O–S mudrock in peripheral area.

range 0.52–0.63, whereas that of the Fe-bearing member decreases from the lower to the middle part, ranging from 0.6 to 0.5. The δEu value varies from 0.65 in the upper part of the Fe-bearing member to 0.7 in the Al-bearing member, and exceeds 0.6 in the O–S mudrock.

5. Discussion

5.1. Eh–pH conditions of bauxite formation

The pH conditions influence Al dissolution and precipitation. Al_2O_3 can dissolve only into ions or complex ions in strongly acidic (pH < 4) or alkaline (pH > 10) solutions (Liao, 1998). However, such conditions rarely exist in nature, where the pH is usually 5–9. Al_2O_3 therefore generally precipitates under neutral conditions and is stable during weathering (Hill et al., 2000; Zhang et al., 2013a, 2013b). La/Y and $(La/Yb)_N$ can be used as geochemical parameters to determine the pH during bauxite formation. La/Y values of >1 and <1 are associated with alkaline and acidic conditions, respectively (Maksimovic and Panto, 1991; Radusinović et al., 2017; Abedini et al., 2018). $(La/Yb)_N$ is lower under acidic conditions and higher under alkaline conditions (Abedini et al., 2018). The La/Y and $(La/Yb)_N$ values in the Yudong profile are characterised by two shifts from high to low (Fig. 13d and e). The first shift occurs from the Fe-bearing member to the middle–lower part of the Al-bearing member, with La/Y and $(La/Yb)_N$ values changing from 1.98 to 2.66 and 8.7–15.93, to 0.23–1.02 and 1–4.41, respectively. The second shift occurs from the aluminous mudstone to the bauxite in the upper part of the Al-bearing member, with La/Y and $(La/Yb)_N$ values decreasing from 2.35 and 9.94, to 0.3–1.02 and 1.32–4.13, respectively. The La/Y and $(La/Yb)_N$ values of the overlying grey–yellow mudrock are 2.06 and 9.44, respectively. These values indicate that the bauxite profile shifted between acidic and alkaline conditions. The bauxite is therefore inferred to have formed under acidic conditions, whereas the aluminous mudstone likely formed under alkaline conditions.

Ce anomalies are reportedly related to redox conditions. Under oxic conditions, Ce^{3+} is transformed to Ce^{4+}, which has a low solubility and is easily precipitated into sediments, resulting in positive anomalies. In contrast, under reduced conditions, Ce is present as soluble Ce^{3+}, resulting in negative anomalies in sediments (Mongelli et al., 2014; Zamanian et al., 2016; Abedini et al., 2018). The samples from the bottom of the Yudong profile have slightly negative Ce anomalies (0.93–0.95), whereas the other samples have positive Ce anomalies (1.07–1.59; Table 1, Fig. 13b). The Ce anomalies are generally higher in the Al-bearing member than in the Fe-bearing member, similarly to the Wuchuan–Zheng'an–Daozhen bauxite deposit (Wang et al., 2013), the Zagrad karstic bauxite deposit, Montenegro (Radusinović et al., 2017), and the Apulian karst bauxite deposit, southern Italy (Mongelli et al., 2014). The change in Ce anomalies suggests that the samples from the bottom formed under reducing conditions, whereas the other samples (including the bauxite) formed under oxic conditions. In conclusion, the

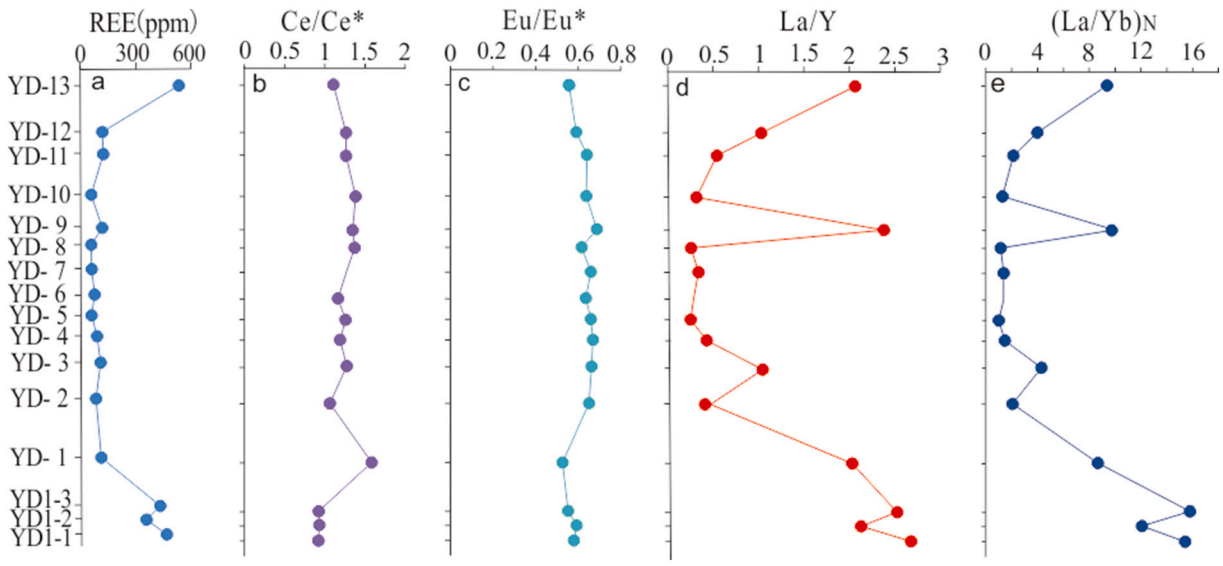

Fig. 13. Variations in (a) total rare earth element content (ΣREE), (b) Ce anomalies, (c) Eu anomalies, (d) La/Y, and (e) $(La/Yb)_N$ in ore-bearing rock series against thickness in Yudong profile.

Yudong bauxite likely formed under acidic oxic conditions, whereas the bauxitic mudrock formed under alkaline reducing conditions.

5.2. Parental affinity

The origins of the karstic-type bauxite in the Kaili–Huangping area remain controversial, and two viewpoints exist. Some researchers have suggested that the bauxite is related to the palaeo-karstification of the bedrock, and the aluminous material originated from the weathering residue of carbonates (Li et al., 2012; Wu et al., 2013; Liu et al., 2014). In contrast, Wang et al. (2018) analysed detrital zircons in the bauxite, which indicated that sedimentary rocks in the central parts of the South China Block were the source of the bauxite. However, neither viewpoint explains the concrete origin of the bauxites, and, to date, geochemical evidence has been lacking. Analytical methods that have previously been used to determine the source of bauxite include immobile element ratios (MacLean and Kranidiotis, 1987; MacLean and Barrett, 1993; Calagari and Abedini, 2007; Zamanian et al., 2016; Yuste et al., 2017), REE patterns (Karadağ et al., 2009; Zamanian et al., 2016), Eu anomalies vs. TiO_2/Al_2O_3 (Mongelli, 1993; Ahmadnejad et al., 2017), Eu anomalies vs. Sm/Nd (Ahmadnejad et al., 2017), and Cr–Ni bivariate plots (Calagari and Abedini, 2007; Ahmadnejad et al., 2017).

5.2.1. Immobile element ratios

Alkali and alkaline earth elements (e.g., K, Na, Ca, and Mg) easily migrate and are depleted during weathering and bauxitisation, without forming secondary minerals (Mordberg, 1996; Hill et al., 2000). However, some trace elements, such as Ti, Zr, Hf, Nb, Ta, Ga, Th, Ni, and Cr, are stable during weathering and bauxitisation (MacLean et al., 1997; Calagari and Abedini, 2007; Radusinović et al., 2017). The ratios of immobile elements (e.g., Nb/Ta and Zr/Hf) in bauxite resemble those in the precursor rocks, owing to the great differences between source regions, which have been used to identify protoliths (MacLean et al., 1997; Calagari and Abedini, 2007; Ahmadnejad et al., 2017). The element correlation diagrams for these elements show linear arrays with strong positive correlations (MacLean et al., 1997). In this study, Nb was found to be positively correlated with Ta, and Zr is positively correlated with Hf, Nb, and Ta (with the correlation line also passing through the O–S mudstone composition), indicating a genetic relationship between the bauxite and the O–S mudrock, with a single homogeneous source. The Ti/Nb, Zr/Hf, and Nb/Ta values of the O–S mudrock and the Gaopochang Formation dolomite are similar to those of the bauxite and the aluminous mudstone (Figs. 10 and 11), indicating that these rocks are related. The O–S mudrock is also strongly correlated with the bauxite and aluminous mudstone (Figs. 10 and 11).

5.2.2. Eu anomalies

Some ratios, especially Eu anomalies, serve as conservative indicators of bauxitisation (Zamanian et al., 2016; Ahmadnejad et al., 2017) and are preserved under strong weathering conditions (Mongelli, 1993; Ahmadnejad et al., 2017). The Eu/Eu* value is an indicator of chemical differentiation (Mongelli et al., 2014) and remains at values similar to those of the source rocks. It is therefore more useful than other origin indicators (Mongelli et al., 2014). This ratio may be useful for identifying bauxite formation (Mameli et al., 2007; Ahmadnejad et al., 2017). The Eu/Eu* values of the O–S mudrock are similar to those of the Al-bearing rocks in the weathering profile, despite a narrower range (Table 1), indicating that the Eu/Eu* values of the rocks are not associated with bauxitisation. The TiO_2/Al_2O_3 ratio has also been used to trace the source rocks of bauxite (Mameli et al., 2007) and is believed to be a sensitive indicator of the source rock characteristics (Mongelli et al., 2014).

The Eu/Eu* value of bauxite (average 0.65) is similar to that of the upper continental crust (average 0.66; Taylor and McLennan, 1985). In the TiO_2/Al_2O_3–Eu/Eu* discrimination diagrams (Fig. 14a), the Eu/Eu* values of the bauxite and bauxitic mudrock are close to those of the O–S mudrock, NASC, and upper continental crust, but different from those of the Gaopochang Formation dolomite and the dolerite and granite in the Fanjingshan area (Guizhou Geological Survey Institute, 2017). These characteristics suggest that the O–S mudrock may represent the source rock of the bauxite and bauxitic mudrock.

Under strong tropical weathering conditions, the fractionation between Sm and Nd is minor. The Sm/Nd ratio, like the Eu/Eu* ratio, may also constitute a useful indicator of chemical differentiation. The Sm/Nd ratio has been used to successfully identify the source rocks of bauxite (Mongelli et al., 2014). The Sm/Nd–Eu/Eu* discrimination diagrams (Fig. 14b) show that the values of the bauxite and bauxitic mudrock are close to those of the NASC, O–S mudrock, and Gaopochang Formation dolomite, but are significantly different from those of the Fanjingshan spilite (Guizhou Geological Survey Institute, 2017). Again, this indicates that the O–S mudrocks may represent the source of the bauxite and bauxitic mudrock, with the Gaopochang Formation dolomite providing a minor amount of material.

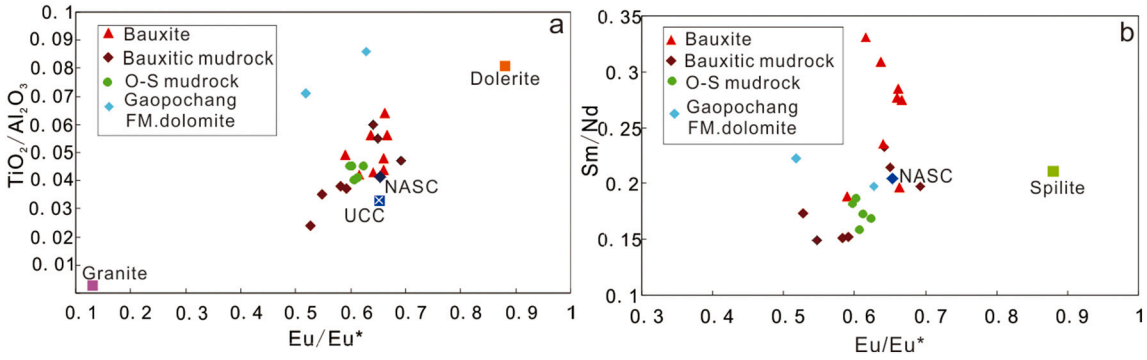

Fig. 14. (a) Discrimination diagrams of TiO_2/Al_2O_3 and Eu/Eu*. Eu/Eu* values of bauxite and bauxitic mudrock were close to those of O–S mudrock, North American shale composite (NASC), and upper continental crust but varied from those of Gaopochang Formation dolomite and Fanjingshan dolerite and granite (Guizhou Geological Survey Institute, 2017). (b) Discrimination diagrams of Sm/Nd and Eu/Eu*. Bauxite and bauxitic mudrock appear similar to the NASC, O–S mudrock, and Gaopochang Formation dolomite and different from Fanjingshan spilite (Guizhou Geological Survey Institute, 2017).

5.2.3. REE distribution patterns

The chondrite-normalised REE patterns of bauxite can be used to identify the source material (Liu et al., 2010; Abedini and Calagari, 2013; Zamanian et al., 2016; Ahmadnejad et al., 2017). Although there are similarities (e.g., LREE characteristics and Eu anomalies) between the O–S mudrock, the bauxite, and the bauxitic mudrock, the HREE characteristics differ significantly (Fig. 12). The HREEs in the O–S mudrock show flat distributions, whereas those in the bauxite and bauxitic mudrock display left-leaning distributions. The Gaopochang Formation dolomite displays the same LREE characteristics and Eu anomalies as the O–S mudrock, the bauxite, and the bauxitic mudrock, but the HREEs display right-leaning distributions. This further suggests that the O–S mudrock may represent the source rock of the bauxite and bauxitic mudrock, with a contribution from the dolomite.

5.2.4. Cr–Ni diagrams

Possible bauxite sources can be traced using the distributions of Cr and Ni in bauxite and bauxitic mudrock (Schroll and Sauer, 1968; Calagari and Abedini, 2007; Radusinović et al., 2017). In the Cr–Ni discrimination diagram (Fig. 15), the ore-bearing rock series plot in the region corresponding to high-iron lateritic bauxite. In addition, the transition regions of the high-iron lateritic, low-iron lateritic, and karst-type bauxites are close to the compositions of shale, slate, and basalt. Considering the regional strata, the source rock of the bauxite and bauxitic mudrock may correspond to the O–S mudrock, namely, the mudrocks of the Wengxiang Group and Dawan Formation.

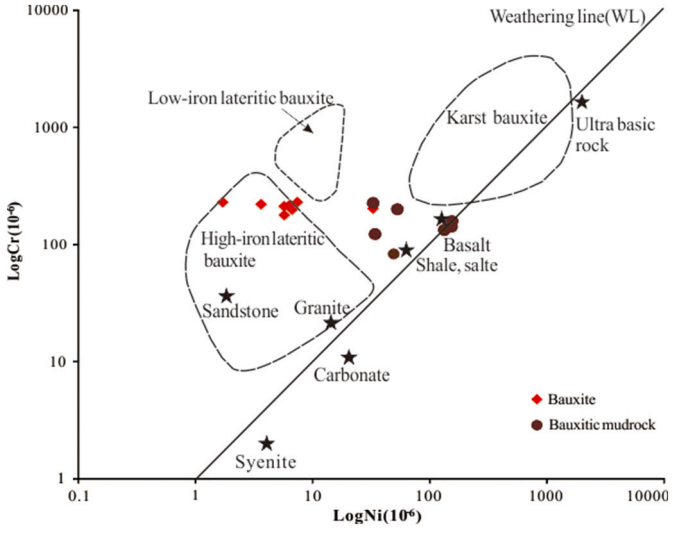

Fig. 15. Cr–Ni discrimination diagrams of ore-bearing rock series in Yudong profile (Schroll and Sauer, 1968).

5.2.5. Comparison with other bauxite deposits

The geochemical characteristics of the Yudong bauxite are compared with those of worldwide bauxite deposits in Table 2. The SiO_2 content of the Yudong bauxite deposit (22.94%) is similar to that of the Wuchuan and Jiagou deposits in China, the Amir-Abad and Siahrudar deposits in Iran, and the Nurra deposit in Italy. However, the SiO_2 content differs from that of the Yunfeng bauxite deposit in China (12.23%), the Apulian deposit in Italy (12.48%), and Zagrad deposit in Montenegro (2.01%). The Al_2O_3 content of the Yudong deposit is similar to that of the Yunfeng and Jiagou bauxite deposits in China, and the Zagrad deposit in Montenegro. The Al_2O_3 contents of the Chinese bauxite deposits are generally much higher than those of Iranian and Italian deposits. The Fe_2O_3 content of the Yudong deposit is similar to that of other bauxite deposits in China, which all have a lower Fe_2O_3 content (2–6%) varying over a wide range (0.5–23%). Furthermore, the bauxite deposits in Iran, Italy, and Montenegro, except the Nurra deposit, have higher Fe_2O_3 content (17–21%) with a narrow range (13–30%). The TiO_2 content (2.74%) of the Yudong bauxite is similar to that of the Yunfeng, Jiagou, Zagrad, Nurra, and Siahrdar deposits (2.21–3.56%). In addition, the TiO_2 content of the Yudong bauxite is higher than that of the Wuchan deposit but lower than that of the Apulian and Amir-Abad deposits. The $\sum$REE of the Yudong deposit (130 ppm) is lower than that of the Chinese bauxite deposits (200–1050 ppm), as well as deposits in Iran, Italy, and Montenegro.

From a review of previous studies, it is clear that the parent rocks of bauxite deposits in Iran and Italy mainly consist of basic magmatic rocks, while those of the Chinese deposits mainly consist of mudrocks. The geochemical characteristics of the Yudong deposit are generally similar to those of other Chinese bauxite deposits, and are close to those of the Zagrad deposits in Montenegro, but differ from the bauxite deposits in Iran and Italy (Table 2). These geochemical characteristics suggest that the parent rocks of the Yudong bauxite deposits mainly consist of mudrock.

5.3. REE behaviour during bauxite mineralisation

The correlation coefficients shown in Table 3 are variable, and indicate both positive and negative correlations. The REEs generally have negative correlations with Al, Ti, P, Zr, and Nb and positive correlations with Si, Fe, K, Na, Mg, Ca, Mn, and Y (Table 3). The LREEs display more positive correlations with Si, K, Na, Mg, Ca, and Mn and more negative correlations with Al, Ti, P, and Zr than the HREEs. The REEs may therefore be related to clay, Fe-bearing, and Y-bearing minerals. The HREEs and Fe in the Yudong bauxite profile are positively

Table 2
Comparison of some characteristics of the Yudong bauxite deposit with some deposits in the world.

Location of bauxite deposits	SiO_2 (wt%)	Al_2O_3 (wt%)	Fe_2O_3 (wt%)	TiO_2 (wt %)	REE (ppm)	Main parent rock	References
Amir-Abad (NW Iran)	13.69–32.01 (22.56)	28.89–51.23 (41.04)	14.65–24.15 (19.85)	3.09–5.95 (4.72)	150.6–932.7 (428.41)	Basaltic rocks	Abedini and Khosravi (2020)
Siahrudar (Northern Iran)	19–31.4 (26.30)	13.97–50.87 (37.57)	13–29.63 (17.94)	1.71–3.56 (2.21)	124.7–723.4 (373.64)	Basalts	Kiaeshkevarian et al. (2020)
Apulian (Italy)	6.79–20.51 (12.48)	39.38–58.46 (47.33)	13.18–28.06 (21.03)	3.42–4.59 (4.4)	152–1167 (550)	Magmatic and clastic material	Mongelli et al. (2014)
Nurra (Italy)	2.1–43.58 24.85	21.89–75.73 (50.64)	1.45–18.82 (8.32)	1.08–3.92 (2.94)	56–2888 (487)	Mafic rocks	Mameli et al. (2007)
Zagrad (Cross-section I, Montenegro)	1–4.63 (2.01)	55.65–61.14 (59.57)	17.82–22.21 (21.29)	2.57–3.19 (2.99)	714.8–5658.4 (1513.22)	Shales	Radusinović et al. (2017)
Jiagou (Henan, China)	1.61–43.26 (15.11)	34.57–78.49 (64.28)	0.51–7.66 (2.6)	1.68–5.06 (3.27)	11.8–964 (282.55)		Zhu et al. (2019)
Wuchuang (Guizhou, China)	1.9–43.6 (32.37)	31.77–71.63 (44.66)	0.6–21.1 (6.17)	0.61–3.06 (1.48)	16.7–806 (198.8)	Mud shales	Gu et al. (2013)
Yunfeng (Guizhou, China)	1.56–24.4 (12.23)	51.1–73.66 (62.73)	1.11–23.49 (4.22)	1.92–5.3 (3.56)	266–2188 (1051)	Dolomite and black rock sequence	Long et al. (2017)
Yudong	0.45–44.77 (22.94)	32.99–80.81 (57.4)	0.62–9.07 (2.25)	0.96–4.24 (2.74)	41.4–486.7 (130.15)	Mudrock	This study

Table 3
Correlation coefficients between the REES and major and trace elements in Yudong profile.

	La	Ce	Pr	Nd	Sm	Eu	Gd	Tb	Dy	Ho	Er	Tm	Yb	Lu
Al_2O_3	−0.65	−0.66	−0.61	−0.60	−0.60	−0.59	−0.55	−0.47	−0.30	−0.21	−0.19	−0.19	−0.02	−0.14
SiO_2	0.61	0.62	0.57	0.55	0.54	0.53	0.48	0.38	0.20	0.10	0.08	0.08	−0.10	0.03
Fe_2O_3	0.44	0.45	0.47	0.48	0.50	0.54	0.54	0.63	0.67	0.67	0.68	0.74	0.65	0.73
TiO_2	−0.68	−0.70	−0.66	−0.65	−0.63	−0.60	−0.56	−0.43	−0.22	−0.08	−0.06	−0.05	0.18	0.07
MgO	0.95	0.94	0.96	0.96	0.96	0.95	0.94	0.88	0.74	0.62	0.89	0.50	0.31	0.34
CaO	0.58	0.57	0.60	0.60	0.59	0.58	0.57	0.53	0.53	0.37	0.33	0.27	0.18	0.15
Na_2O	0.26	0.24	0.26	0.27	0.27	0.28	0.29	0.27	0.29	0.25	0.24	0.21	0.20	0.22
K_2O	0.95	0.95	0.96	0.96	0.96	0.95	0.93	0.85	0.70	0.57	0.54	0.45	0.25	0.29
P_2O_5	−0.65	−0.66	−0.61	−0.60	−0.58	−0.55	−0.51	−0.37	−0.18	−0.04	−0.01	0.01	0.23	0.13
MnO	0.86	0.85	0.87	0.87	0.87	0.86	0.84	0.77	0.66	0.53	0.51	0.44	0.24	0.29
Y	0.64	0.62	0.69	0.70	0.73	0.77	0.81	0.93	0.99	0.99	0.99	0.95	0.88	0.88
Zr	−0.71	−0.72	−0.68	−0.67	−0.65	−0.62	−0.58	−0.42	−0.19	−0.03	−0.01	0.03	0.27	0.18
Nb	−0.65	−0.65	−0.61	−0.59	−0.58	−0.55	−0.51	−0.38	−0.15	−0.02	−0.00	−0.01	0.23	0.11

correlated (R = 0.54–0.74), indicating that Fe oxides and hydroxides played an important role in the preferential enrichment of the HREEs. The REEs, especially the HREEs (R = 0.81–0.99), exhibit positive correlations with Y (R = 0.62–0.99), indicating that they may be related to Y-bearing minerals.

The geochemical characteristics of the Yudong bauxite profile reveal that ΣREE increases from top to bottom (Table 1). Similarly, Fig. 13a shows that the sample REEs are gradually enriched in the lower part of the profile. The pH is a crucial factor affecting REE migration (Nesbitt, 1979; Karadağ et al., 2009). REEs easily migrate from the weathering profile under acidic conditions, but are absorbed by minerals under neutral to alkaline conditions (Nesbitt, 1979; Karadağ et al., 2009; Ahmadnejad et al., 2017). The La/Y (Fig. 13d) and $(La/Yb)_N$ (Fig. 13e) ratios indicate that acidic conditions were dominant during the formation of the Al-bearing member, whereas alkaline conditions were prevalent during the formation of the Fe-bearing member. In addition, the REE content was enriched at the bottom of the weathering profile due to the lack of an adequate active drainage system, and because of the geochemical barriers of the pedestal rock, which consisted of dolomite (Mordberg, 1996).

5.4. Bauxite formation

The bauxite formation in the study area was controlled by earlier tectonic activity. The mining area is located in the centre of the Qianzhong Ancient Fault zone, south of the Huangping–Zhenyuan Fault and north of the Guiyang–Sansui Fault (Fig. 1b). The tectonic activity of these two faults resulted in a complex process of subsidence and uplift in the bauxite area. The Guangxi tectonic activity, which occurred from the end of the Silurian to the beginning of the Devonian, uplifted the area north of the Huangping–Zhenyuan fault. This area was then subjected to long-term weathering. In addition, the Guangxi tectonic activity caused the area south of the Huangping–Zhenyuan fault to subside, resulting in deposition during the Devonian. Consequently, the Gaopochang Formation was exposed in the ore-concentrated area and formed the bottom layers of the ore-bearing rock series. The Ziyun tectonic activity, which occurred from the end of the Devonian to the beginning of the Carboniferous, uplifted the area north of the Guiyang–Sansui Fault, resulting in an absence of sediments and the creation of a karst weathering surface in the Gaopochang Formation dolomite, allowing for the accumulation of the ore-bearing rock series. The Qiangui tectonic activity in the Early to Middle Permian caused the bauxite area to subside relative to the area north of the Huangping–Zhenyuan Fault, resulting in the deposition of sediments from the Liangshan period in the Middle Permian. Bauxite formation thus occurred in three stages: laterisation; migration and precipitation; and, diagenesis and supergene enrichment.

5.4.1. Laterisation stage

During bauxite formation, lateritic weathering is an important metallogenic mechanism by which soil forms at an early stage and aluminous material forms at a later stage in the mineralisation. Appropriate conditions for bauxite formation existed in the study area. First, and most importantly, the area experienced a long period of weathering and denudation. The area north of the Huangping–Zhenyuan Fault, that is, the northern part of the ore collection area, underwent long-term weathering and denudation from the Devonian to the end of the Early

Permian. In this process, the O–S mudrock underwent laterisation, and the laterisation products provided sufficient material for bauxite formation. The ore accumulation area also experienced weathering and denudation from the Carboniferous to the Early Permian, during which a karst unconformity surface formed in the Gaopochang Formation dolomite, allowing for the accumulation of the ore-bearing rock series along with a small amount of dolomite residue. Second, the study area experienced hot and humid climatic conditions as it was located in a low-latitude region. The Guizhou line in the Yangtze Block was located at approximately 10°S during the Devonian, in a warm and humid tropical climate zone (Zeng et al., 1993), and Guizhou was located in a tropical region at 8–14°S during the Carboniferous (Wang and Li, 1998). These paleogeographic and paleoclimatic conditions supported bauxite formation. Third, the geological conditions in the study area were relatively stable. The Guangxi, Ziyun, and Qiangui episodes of tectonic activity north of the Huangping–Zhenyuan Fault were epeirogenic and characterised mainly by the slow rise of the crust, which created ideal conditions for bauxite formation. As a result of long-term weathering, the study area developed a peneplain, forming a lateritic weathering crust containing gibbsite-type bauxite. The differential uplift and subsidence, along with weaker denudation resulting from the slow rise of the crust, preserved the lateritic weathering crust.

5.4.2. Migration and precipitation stage

The lateritic crust in the area north of the Huangping–Zhenyuan Fault was formed by long-term weathering. The material forming the crust was transported by surface runoff to the karst depression and troughs by alluvial–diluvial activity in the early stages of the Middle Permian. During migration, both chemical and mechanical processes occurred, resulting in the leaching of Fe and Si, and the enrichment of Al. Following deposition, the transported material was transformed into stacked lateritic layers, along with a small amount of dolomite weathering residue from the Gaopochang Formation. The stacked lateritic layers were well preserved because of the overlying sedimentary cover.

5.4.3. Diagenesis and supergene enrichment stages

The stacked lateritic layers underwent a series of compaction, consolidation, and other diagenetic processes, causing the gibbsite to transform into diaspore, and forming the original bauxite ore bed. During the Yanshan and Himalayan episodes of tectonic activity, the original bauxite was uplifted to or near the surface. Under the eluviation of the reduction and oxidation zones, Si and Fe dissolved and migrated, and Al, Ti, and other stable elements were enriched again, resulting in the formation of an ancient weathered crust containing secondary sedimentary bauxite. During this process, some elements in the upper profile, such as REEs, were dissolved due to the leaching of acidic surface water, and migrated to the lower part of the profile where they were consolidated because of the geochemical barriers of the carbonate rock.

6. Conclusions

The Al, Ti, V, Cr, Zr, Nb, Hf, Th, and U contents were found to generally increase from the O–S mudrock to the Fe-bearing member, and further increase into the Al-bearing member, whereas the Si, Fe, Rb, Cs, and Ba contents decrease. These characteristics indicate that bauxitisation involved elemental variation. The positions of the sample compositions in the Al_2O_3–Fe_2O_3–SiO_2 ternary plot, the CIA, and the strong positive correlations of some stable elements (such as Al, Ti, Zr, Hf, Nb, and Ta) indicate that the degree of weathering increases gradually from the O–S mudrock to the bauxitic mudrock, and further increases into the bauxite, suggesting that the bauxitic mudrock and bauxite originated from the O–S mudrock.

The La/Y and $(La/Yb)_N$ values reflect differences in pH, and the Ce anomalies are associated with redox conditions. The La/Y values, $(La/Yb)_N$ values, and Ce anomalies indicate that the Yudong bauxite formed under acidic oxic conditions, whereas the bauxitic mudrock formed under alkaline reducing conditions. Analyses of immobile elements, Eu anomalies, REE patterns, and the Cr–Ni diagram show that the ore-bearing rock series originated mainly in the O–S mudrock, with some contribution from the Gaopochang Formation dolomite. Correlation analyses show that the REEs have negative correlations with Al, Ti, P, Zr, and Nb and positive correlations with Si, Fe, K, Na, Ca, Mg, and Y. These results indicate that the REEs may be associated with clay, iron-bearing, and Y-bearing minerals.

The northern part of the ore collection area (the area north of the Huangping-Zhenyuan Fault), underwent long-term weathering and denudation from the Devonian to the end of the Early Permian. The ore accumulation area also experienced weathering and denudation from the Carboniferous to the Early Permian, during which a karst unconformity surface formed in the Gaopochang Formation dolomite. The laterisation products of the O–S mudrock in the northern part of the ore collection area were transported to the karst depression in the early stages of the Middle Permian. The weathering products of the O–S mudrock, with small amounts of the Gaopochang Formation dolomite, accumulated on the karst interface, forming the original bauxite layers during cycles of compaction and concretion. These bauxite layers were uplifted to or near the surface during the Late Cretaceous to Paleogene, eventually, forming karstic bauxite.

Declaration of competing interest

This manuscript has not been published or presented elsewhere in part or in entirety, and it is not under consideration by another journal. All the authors have approved the manuscript and agree with submission to your esteemed journal. There are no conflicts of interest to declare.

Acknowledgments

This work was supported through the United Foundation of National Natural Science Foundation of China (U181240004), through the National Natural Science Foundation of China (41972095, 41830432) and through the Science Foundation of Guizhou Province ([2017]1194). The language of the manuscript is polished by the Elsevier Language Editing Service. We are also grateful to Eimear Deady and an anonymous reviewer, whose constructive comments and suggestions greatly improved this manuscript.

References

Abedini, A., Calagari, A.A., 2013. Rare earth elements geochemistry of Sheikh-Marul laterite deposit, NW Mahabad, West-Azarbaidjan province, Iran. Acta Geol. Sin. 87, 176–185.
Abedini, A., Khosravi, M., 2020. Geochemical constraints on the Triassic-Jurassic Amir-Abad Karst-type bauxite deposit, NW Iran. J. Geochem. Explor. 211, 106489.
Abedini, A., Calagari, A.A., Azizi, R.M., 2018. The tetrad-effect in rare earth elements distribution patterns of titanium-rich bauxites: evidence from the Kanigorgeh deposit, NW Iran. J. Geochem. Explor. 186, 129–142.
Abedini, A., Khosravi, M., Calagari, A.A., 2019. Geochemical characteristics of the Arbanos karst-type bauxite deposit, NW Iran: implications for parental affinity and factors controlling the distribution of elements. J. Geochem. Explor. 200, 249–265.
Ahmadnejad, F., Zamanian, H., Taghipour, B., Zarasvandi, A., Buccione, R., Ellahi, S.S., 2017. Mineralogical and geochemical evolution of the Bidgol bauxite deposit, Zagros Mountain Belt, Iran: implications for ore genesis, rare earth elements fractionation and parental affinity. Ore Geol. Rev. 86, 755–783.
Bárdossy, G., 1989. Bauxite. In: Dev. Earth Surf. Process, vol. 1. Elsevier, Amaterdam, pp. 339–418.
Bogatyev, B.A., Zhukov, V.V., Tsekhovsky, Y.G., 2009. Formation conditions and regularities of the distribution of the large and superlarge bauxite deposits. Lithol. Miner. Resour. 44, 135–151.
Bogatyrev, B.A., Zhukov, V.V., 2009. Bauxite provinces of the World. Geol. Ore Depos. 51, 339–355.
Boynton, W.V., 1984. Geochemistry of the rare earth elements: meteorite studies. In: Henderson, P. (Ed.), Rare Earth Element Geochemistry. Elsevier, pp. 63–114.
Calagari, A.A., Abedini, A., 2007. Geochemical investigations on Permo-Triassic bauxite horizon at the Kanisheeteh, East of Bukan, West-Azarbaidjan, Iran. J. Geochem. Explor. 94, 1–18.

Dong, J.L., 2004. Geological feature of bauxite in Guizhou province and thoughts of exploration & development. Miner. Resour. Geol. 18 (6), 555–558 (in Chinese with English abstract).
Geological Survey of Guizhou Province, 2017. Regional Geology of China-Guizhou Province. Geological Publishing House, Beijing, pp. 1–1153 (in Chinese with English abstract).
Gromet, L.P., Dymek, R.F., Haskin, L.A., Korotev, R.L., 1984. The "North American shale composite": its compilation, major and trace element characteristics. Geochim. Cosmochim. Acta 48, 2469–2482.
Gu, J., Huang, Z.L., Fan, H.P., Jin, Z.G., Yan, Z.F., Zhang, J.W., 2013. Mineralogy, geochemistry, and genesis of lateritic bauxite deposits in the Wuchuan-Zheng'an-Daozhen area, Northern Guizhou Province, China. J. Geochem. Explor. 130, 44–59.
Guizhou Bureau of Geology and Mineral Resources, 1987. Regional Geology of Guizhou Province. Geological Publishing House, Beijing, pp. 1–698 (in Chinese with English abstract).
Guizhou Bureau of Geology and Mineral Resources, 1992. Atlas of Lithofacies and Paleogeography of Guizhou (Mesoproterozoic to Triassic). Science and Technology Publishing House of Guizhou, China, Guiyang, pp. 1–77 (in Chinese with English abstract).
Hill, I.G., Worden, R.H., Meighan, I.G., 2000. Geochemical evolution of a palaeolaterite: the Interbasaltic Formation, Northern Ireland. Chem. Geol. 166 (1–2), 65–84.
Karadağ, M.M., Küpeli, Ş., Arýk, F., Ayhan, A., 2009. Rare earth element (REE) geochemistry and genetic implications of the Mortaş bauxite deposit (Seydişehir/Konya-Southern Turkey). Chem. Erde-Geochem. 69 (2), 143–159.
Kiaeshkevarian, M., Calagari, A.A., Ali, Abedini, Shamanian, G., 2020. Geochemical and mineralogical features of Karst bauxite deposite from the Alborz Zonr (Northern Iran): implication for conditions of formation, behavior of trace and rare earth elements and parental affinity. Ore Geol. Rev. 125, 103691.
Kong, L., Li, C.B., Zhang, J.W., Chu, X.S., Cai, X.D., Liu, Y.P., Wu, G.H., 2013. Geomorphic characteristics of the palaeo-karst and its ore-controlling process on the bauxite deposit in the Kaili-Huangping area, southeastern Guizhou. Miner. Explor. 4 (6), 624–629 (in Chinese with English abstract).
Li, C.B., Liu, Y.P., Wu, G.H., Han, R.S., Cai, X.D., Ma, R., 2012. Ore-controlling factors of the bauxite deposites in the Kaili area, Guizhou province. Geol. Explor. 48 (1), 0031–0037 (in Chinese with English abstract).
Li, C.B., Liu, Y.P., Wu, G.H., Cai, X.D., 2013. Geological characteristics and metallogenic regularity of bauxite deposits in Kaili-Huangping district, Guizhou Province. Miner. Resour. Geol. 27 (1), 45–51 (in Chinese with English abstract).
Liao, S.F., 1998. A new review in genesis and classification of bauxites. Guizhou Geol. 15 (2), 139–144 (in Chinese with English abstract).
Ling, K.Y., Zhu, X.Q., Tang, H.S., Du, S.J., Gu, J., 2018. Geology and geochemistry of the Xiaoshanba bauxite deposit, Central Guizhou Province, SW China: implication for the behavior of trace and rare earth elements. J. Geochem. Explor. 190, 170–186.
Liu, X.F., Wang, Q.F., Deng, J., Zhang, Q.Z., Sun, S.L., Meng, J.Y., 2010. Mineralogical and geochemical investigations of the Dajia Salento-type bauxite deposits, western Guangxi, China. J. Geochem. Explor. 105 (3), 137–152.
Liu, Y.P., Li, C.B., Zhou, W.L., Cai, X.D., Ren, Y.L., 2014. The relationship between spatial distribution of bauxite deposit and ancient karst landform in Kaili-Huangping area, Guizhou province. Sci. Technol. Eng. 14 (31), 165–171 (in Chinese with English abstract).
Long, Y.Z., Chi, G.X., Liu, J.P., Jin, Z.G., Dai, T.G., 2017. Trace and rare earth elements constraints on the sources of the Yunfeng paleo-karstic bauxite deposit in the Xiuwen-Qingzhen area, Guizhou, China. Ore Geol. Rev. 91, 404–418.
MacLean, W.H., Barrett, T.J., 1993. Lithogeochemical techiques using immobile elements. J. Geochem. Explor. 84, 109–133.
MacLean, W.H., Kranidiotis, P., 1987. Immobile elements as monitors of mass transfer in hydrothermal alteration: Phelps Dodge massive sulfide deposit, Matagami, Quebec. Econ. Geol. 82, 951–962.
MacLean, W.H., Bonavia, F.F., Sanna, G., 1997. Argillite debris converted to bauxite during karst weathering: evidence from immobile element geochemistry at the Olmedo Deposit, Sardinia. Mineral. Deposita 32, 607–616.
Maksimovic, Z., Panto, Gy, 1991. Contribution to the geochemistry of the rare earth elements in the karsit-bauxite deposits of Yugoslavia and Greece. Geoderma 51, 93–109.
Mameli, P., Mongelli, G., Oggiano, G., Dinelli, E., 2007. Geological, geochemical and mineralogical features of some bauxite deposits from Nurra (Western Sardinia, Italy): insights on conditions of formation and parental affinity. Int. J. Earth Sci. 96 (5), 887–902.
Mongelli, G., 1993. REE and other trace elements in a granitic weathering profile from "Serre", southern Italy. Chem. Geol. 103, 17–25.
Mongelli, G., Boni, M., Buccione, R., Sinisi, R., 2014. Geochemistry of the Apulian karst bauxites (southern Italy): chemical fractionation and parental affinities. Ore Geol. Rev. 63, 9–21.
Mordberg, L.E., 1996. Geochemistry of trace elements in Paleozoic bauxite profiles in northern Russia. J. Geochem. Explor. 57, 187–199.
Nesbitt, H.W., 1979. Mobility and fractionation of rare earth elements during weathering of a granodiorite. Nature 297, 206–210.
Nesbitt, H.W., Young, G.M., 1982. Early Proterozoic climates and plate motions inferred from major element chemistry of lutites. Nature 299, 715–717.
Qi, L., Hu, J., Gregoire, D.C., 2000. Determination of trace elements in granites by inductively coupled plasma spectrometry. Talanta 51, 507–513.
Radusinović, S., Jelenković, R., Pačevski, A., Simić, V., Božović, D., Holclajtner-Antunović, I., Životić, D., 2017. Content and mode of occurrences of rare earth elements in the Zagrad karstic bauxite deposit (Nikšić area, Montenegro). Ore Geol. Rev. 80, 406–428.
Schellmann, W., 1986. A new definition of laterite. In: Memoirs of the Geological Survey of India, vol. 120, pp. 1–7.
Schroll, E., Sauer, D., 1968. Beiträge zur Geochemie von Titan, Chrom, Nickel, Cobalt, Vandium und Molybdän in bauxitishcen Gesteinen und das Problem der stoffichen Herkunft des Alumniums. Travax du l'ICSOBA 5, 83–96.
Taylor, S.R., McLennan, S.M., 1985. The Continental Crust: Its Composition and Evolution. Blackwell, Oxford, pp. 1–312.
Wang, J.D., Li, H.M., 1998. Carboniferous paleo-latitude and bauxite deposit of Central Guizhou Provence. Geochimica 27 (6), 575–578 (in Chinese with English abstract).
Wang, X.M., Jiao, Y.Q., Du, Y.S., Ling, W.L., Wu, L.Q., Cui, T., Zhou, Q., Jin, Z.G., Lei, Z. Y., Weng, S.F., 2013. REE mobility and Ce anomaly in bauxite deposit of WZD area, Northern Guizhou, China. J. Geochem. Explor. 133, 103–117.
Wang, R.X., Wang, Q.F., Huang, Y.X., Yang, S.J., Liu, X.F., Zhou, Q., 2018. Combined tectonic and paleogeographic controls on the genesis of bauxite in the Early Carboniferous to Permian Central Yangtze Island. Ore Geol. Rev. 101, 468–480.
Wu, Z.T., Wu, L., Tian, H.D., Wu, G., 2013. Metallogenic relation between deposit in Huangping of Kaili and ancient karst. Guizhou Geol. 30 (2), 90–94 (in Chinese with English abstract).
Ye, L., Pan, Z.P., Cheng, Z.T., 2007. The prospects of comprehensive utilization of associated elements in bauxites from Guizhou. Acta Miner. Sinica 27 (3/4), 388–392 (in Chinese with English abstract).
Yuste, A., Bauluz, B., Mayayo, M.J., 2017. Origin and geochemical evolution from ferrallitized clays to karst bauxite: an example from the Lower Cretaceous of NE Spain. Ore Geol. Rev. 84, 67–79.
Zamanian, H., Ahmadnejad, F., Zarasvandi, A., 2016. Mineralogical and geochemical investigations of the Mombi bauxite deposit, Zagros Mountains, Iran. Chem. Erde Geochem. 76, 13–37.
Zeng, Y.F., zhang, J.Q., Liu, W.J., Zhou, H.L., Chen, H.D., 1993. Devonian Lithofacies, Paleogeoragraphy and Mineralization in South China. Geological Publishing House, Beijing, pp. 1–123 (in Chinese with English abstract).
Zhang, Z.W., Li, Y.J., Zhou, L.J., Wu, C.Q., 2012. Coal-bauxite-iron structure and geochemical features of bauxites ore-bearing rock series in southeast Guizhou. Acta Geol. Sin. 86 (07), 1119–1131 (in Chinese with English abstract).
Zhang, G.W., Guo, A.L., Wang, Y.J., Li, S.Z., Dong, Y.P., Liu, S.F., He, D.F., Cheng, S.Y., Liu, R.K., Yao, A.P., 2013a. Tectonics of South China continent and its implications. Sci. China-Earth Sci. 56 (11), 1804–1828.
Zhang, Z.W., Zhou, L.J., Li, Y.J., Wu, C.Q., Zheng, C.F., 2013b. The "coal-bauxite-iron" structure in the ore-bearing rock series as a prospecting indicator for southeastern Guizhou bauxite mines. Ore Geol. Rev. 53, 145–158.
Zhu, K.Y., Su, H.M., Jiang, S.Y., 2019. Mineralogical control and characteristics of rare earth elements occurrence in Carboniferous bauxites from western Henan Province, north China: a XRD, SEM-EDS and LA-ICP-MS analysis. Ore Geol. Rev. 114, 103144.